processes

MDPI

Article

Amomum subulatum Fruit Extract Mediated Green Synthesis of Silver and Copper Oxide Nanoparticles: Synthesis, Characterization, Antibacterial and Anticancer Activities

Sarika Dhir [1,*], Rohit Dutt [1], Rahul Pratap Singh [1], Mahima Chauhan [1], Tarun Virmani [2,*], Girish Kumar [2], Abdulsalam Alhalmi [3], Mohammed S. Aleissa [4], Hassan A. Rudayni [4] and Mohammed Al-Zahrani [4]

1 Department of Pharmacy, School of Medical & Allied Sciences, G.D. Goenka University, Gurugram 122103, Haryana, India; rohitdatt23@rediffmail.com (R.D.); anuraza2009@gmail.com (R.P.S.); mahimachauhan708@gmail.com (M.C.)
2 School of Pharmaceutical Sciences, MVN University, Palwal 121105, Haryana, India; girish.kumar@mvn.edu.in
3 Department of Pharmaceutics, School of Pharmaceutical Education and Research, Jamia Hamdard, New Delhi 110062, Delhi, India; asalamahmed5@gmail.com
4 Biology Department, College of Science, Imam Mohammad Ibn Saud Islamic University (IMSIU), Riyadh 11623, Saudi Arabia; msaleissa@imamu.edu.sa (M.S.A.); harudayni@imamu.edu.sa (H.A.R.); mmyalzahrani@imamu.edu.sa (M.A.-Z.)
* Correspondence: sarikadhir_22@yahoo.co.in (S.D.); tarun.virmani@mvn.edu.in (T.V.)

Abstract: This research presents a straightforward, effective, and eco-friendly method for the production of silver nanoparticles (AgNPs) and copper oxide nanoparticles (CuONPs) using the dried fruit of *Amomum subulatum* as a reducing, stabilizing, and capping agent. The formation of AgNPs and CuONPs is supported by the presence of a surface plasmon resonance band (SPR) at 440 nm for AgNPs and 245 nm for CuONPs. Additionally, the identification of specific biomolecules responsible for the synthesis of AgNPs and CuONPs was confirmed through FTIR spectra analysis. The Transmission electron microscope (TEM) images demonstrated that AgNPs and CuONPs had spherical shapes, with mean particle diameters of 20.6 nm and 24.7 nm, respectively. X-ray diffraction and selected area electron diffraction (SAED) analyses provided evidence of the crystalline nature of the synthesized AgNPs and CuONPs. Additionally, the presence of silver and copper elements was observed through energy-dispersive X-ray spectroscopy (EDS) analysis. Furthermore, the antibacterial activity of AgNPs was found to be superior to that of CuONPs against human pathogens such as *Escherichia coli*, *Staphylococcus aureus*, and *Bacillus subtilis*. The cytotoxic activity of the biosynthesized nanoparticles (NPs) was evaluated in vitro against human cervical cells (HeLa) and human breast cells (MCF-7). In MCF-7 cells, the IC_{50} value for AgNPs was estimated to be 39.79 µg/mL, while that of CuONPs was 83.89 µg/mL. In HeLa cells, the IC_{50} value for AgNPs was 45.5 µg/mL, and for CuONPs, it was 97.07 µg/mL. For the first time, an eco-friendly method for the synthesis of AgNPs and CuONPs from fruit extract of *Amomum subulatum* has been discussed along with their comparative evaluation study. These results highlight the promising applications of the eco-friendly synthesized AgNPs and CuONPs as effective agents against microbial infections and potential candidates for cancer therapy.

Keywords: *Amomum subulatum*; silver NPs; copper oxide NPs; antibacterial activity; anticancer activity

Citation: Dhir, S.; Dutt, R.; Singh, R.P.; Chauhan, M.; Virmani, T.; Kumar, G.; Alhalmi, A.; Aleissa, M.S.; Rudayni, H.A.; Al-Zahrani, M. *Amomum subulatum* Fruit Extract Mediated Green Synthesis of Silver and Copper Oxide Nanoparticles: Synthesis, Characterization, Antibacterial and Anticancer Activities. *Processes* **2023**, *11*, 2698. https://doi.org/10.3390/pr11092698

Academic Editors: Jelena D. Vujančević and Zorka Z. Vasiljevic

Received: 7 July 2023
Revised: 1 September 2023
Accepted: 2 September 2023
Published: 9 September 2023

1. Introduction

In recent years, microorganisms, mainly *Staphylococcus aureus* (*S. aureus*) and *Escherichia coli* (*E. coli*), have become more resilient to various antimicrobial treatments causing serious health concerns for humans [1,2].

Similarly, cancer is the second leading cause of mortality across the globe, accounting for 7.6 million deaths, with the number expected to climb to almost 13.1 million by 2030 [3,4]. Surgery, radiation, chemotherapy, and a combination of these treatments are the

mainstays of traditional treatment, and chemotherapeutic treatment is widely accepted for the treatment of cancer. However, chemotherapeutic treatment suffers from various hindrances of adverse effects, drug resistance, absence of targeting, insensitivity of cancer cells to drugs, and patient incompliance, which must be combated for efficacious treatment of cancer [5,6].

To deal with these issues related to microbial treatment and cancer, nanoparticles have gained attention owing to their nano size, a higher ratio of surface area to surface volume, chemical, magnetic, optical, and mechanical properties, safety, improved stability, and cost-effectiveness [7,8]. Nanoparticles based on metal or metal oxide, such as silver, gold, copper, titanium, zinc, etc., have promising outcomes for various biomedical applications due to the possession of multifunctional theranostic facilities [9,10]. Metal/Metal oxide nanoparticles (NPs) possess distinctive physical, chemical, and biological properties compared to their bulk form primarily due to their large surface area to volume ratio. This characteristic makes them highly attractive for various applications [11].

Various physical, chemical, and biological methods like chemical reduction, electrochemical reduction, sonication, thermal decomposition, and enzymatic decomposition are employed to fabricate metal/metal oxide nanoparticles, having their own limitations like requirement of toxic materials, the greater amount of energy, solvent, and labor [12,13]. To address these concerns, researchers are actively exploring plant-based manufacturing of nanoparticles, namely green synthesis, due to reduced toxicity, eco-friendliness, low time consumption, and cost-effectiveness. Plants contain various phytoconstituents, namely alkaloids, tannins, glycosides, flavonoids, aldehydes, ketones, polyphenols, aldehydes, amines, etc., which serves as reducing, capping, and stabilizing agent in the translation of metal ions into metallic nanoparticles having presumed properties [14,15].

Amomum subulatum, which is commonly known as Black cardamom or Badi Elaichi, belongs to the *Zingiberaceae* family and has dark brown pods with tough, dried skin. It is easily available, cost-effective, and possesses various phytochemical constituents *such as* carbohydrates, proteins, flavonoids, phenolics, terpenoids, steroids, glycosides, tannins, alkaloids, fixed oil, and fats [16]. The presence of polyphenols and flavonoids provides antioxidant properties, due to which it can be employed as a reducing, stabilizing agent, or both in the translation of metal ions into metallic nanoparticles [17]. Additionally, the polyphenolic compounds, flavonoids, and proteins from the aqueous extract of *Amomum subulatum* get adsorbed on the surface of the CuONPs and AgNPs and act as capping agents causing a synergistic effect in biological activities of these metal NPs [18]. Despite the possession of numerous phytoconstituents responsible for reduction or stabilization, *Amomum subulatum* has limited research as a reducing, stabilizing, and capping agent in the fabrication of metal/metal ion nanoparticles. Hence, in this study, *Amomum subalatum* was chosen to prepare the AgNPs and CuONPs.

Amongst numerous green synthesized nanoparticles, CuONPs and AgNPs have risen to the top in the last two decades as a result of their distinctive biological, chemical, and physical characteristics [19]. Numerous studies have utilized extracts from various plant species for the synthesis of AgNPs and CuONPs and assessed their antibacterial, antioxidant, and anticancer activities. Some examples include the use of extracts from *Sphaeranthus indices* [20], *Acalypha indica* [21], *Salvia spinosa* [22], *Pinus roxburghii* [23], *Camellia sinensis* [24], *Eucalyptus globulus* [25], *Azadirachta indica* [26], *Sida acuta* [27]. These studies demonstrated the potential of plant-based synthesis of nanoparticles and highlighted their antioxidant, antibacterial, and anticancer properties.

Hence, in this study, CuONPs and AgNPs were fabricated using the fruit extract of *Amomum subalatum* as a reducing or stabilizing agent to provide antibacterial and anticancer potential.

2. Materials and Methods

2.1. Materials

The *Amomum subulatum* fruits were obtained from a local marketplace in Faridabad, Haryana. The authenticity of these fruits was confirmed by Dr. Sunita Garg at the National Institute of Science Communication and Information Resources (NISCAIR) under reference number NISCAIR/RHMD/CONSULT/2020/3766-67-2. Reagents utilized in the study were procured from CDH (Central Drug House) and Fine Chemicals in Delhi, India unless explicitly stated otherwise. Tryptone broth and Soybean Casein Digest Agar (SCDA) were sourced from HiMedia Laboratories Pvt. Ltd. in Mumbai. All chemicals were employed in their original form without undergoing additional purification processes.

2.2. Preparation of Amomum Subulatum Fruit Extract

Before starting the experiment, a preliminary procedure was performed on *Amomum subulatum* fruits. This involved several washes with distilled water. The fruits were then air-dried under shaded conditions at room temperature until completely dried. After drying, the fruits turned into a coarse powder. To form the aqueous extract, 5 g of ground fruit material was carefully placed in a vessel containing 100 mL of distilled water. This mixture was then left to stand at room temperature for 24 h to facilitate extraction. After the prescribed time, the mixture was filtered using a special filter paper known as Whatman No. 1 (11 µm, Sigma Aldrich, Bangalore, India). This filtration step was crucial to separate the solid and liquid components and extract the desired extract. The resulting extract was then safely stored at 4 °C. This preservation was conducted to preserve the integrity and quality of the extract and ensure its suitability for future use. The preserved extract was reserved for its role in the synthesis of silver and copper oxide nanoparticles, which represented an important step in the experimental process.

2.3. Qualitatively Preliminary Phytochemical Analysis of the Extract

The initial qualitative phytochemical analysis of the aqueous extract of *Amomum subulatum* fruit included the determination of the main phytochemical components. These components included alkaloids, tannins, saponins, flavonoids, glycosides, proteins, carbohydrates, phenols, amino acids and terpenoids. The analysis was performed using established methods documented in the available literature.

2.3.1. Test for Primary Metabolites

Molisch's Test: To do the Molisch Test, we added 2 to 3 drops of the Molisch reagent to our extracts. We let the mixture mix for a while. Then, we carefully added a concentrated amount of hydrogen sulfoxide to the inside walls of our test tube. When the two liquids came together, we saw a violet ring. That meant there were carbohydrates in the mixture!

Million's test: 5 mL Million's reagent (mercury + nitric acid + distilled water) was added to the extract solution; red color indicates a positive test for proteins [28].

2.3.2. Test for Secondary Metabolites

Shinoda test: The application of the Shinoda Test commenced with the introduction of 5 mL of 95% ethanol into the extracts. Following this step, a small quantity of concentrated hydrochloric acid (HCl) was carefully added, along with the inclusion of 0.5 g of magnesium turnings. The conclusive indication of the presence of flavonoids was signaled by the emergence of precipitates with a distinct pink hue [28].

Dragendorff's Test: A few drops of Dragendorff's reagent (Sodium iodide + basic bismuth carbonate + glacial acetic acid) were added to the extract. Orange-brown precipitates indicate the presence of alkaloids [29].

Foam Test: The Foam Test includes aggressively stirring the extract with water, resulting in persistent foam production. This froth production is conclusive evidence of saponin content in the tested extract [30].

The Keller–Killani test was executed by treating a 2 mL extract with a combination of glacial acetic acid, 5% $FeCl_3$, and concentrated H_2SO_4. The presence of glycosides becomes apparent through the manifestation of a reddish-brown shade at the juncture where two liquid layers meet, accompanied by an upper layer displaying a blue-green coloration [29].

The Ferric chloride ($FeCl_3$) test involved adding a small number of drops of a 5% $FeCl_3$ solution to the extract. The confirmation of the presence of tannins and phenols is established when a profound blue-black color develops as a result of this reaction [31].

The Salkowski Test was performed by mixing 2 mL of the extract with 2 mL of chloroform and 3 mL of concentrated H_2SO_4, which resulted in the creation of a distinct monolayer. When a reddish-brown coloring arises at the interface of the two layers, this confirms the existence of terpenoids [28].

Ninhydrin test (general test): 3 mL extract and 3 drops of 5% Ninhydrin solution were heated in a boiling water bath for 10 min. The purple or bluish color indicates the presence of amino acids [29].

2.4. Preparation of Metal Solutions

Different concentrations (1 mM, 3 mM, and 5 mM) of $AgNO_3$ and (0.05 M, 0.1 M, 0.2 M) of $CuSO_4 \cdot 5H_2O$ solutions were prepared by dissolving (0.017 g, 0.051 g, 0.085 g of silver nitrate each separately in 100 mL of distilled water) and (1.25 g, 2.5 g, 5 g of copper sulfate pentahydrate each in 100 mL of distilled water). The volumetric flasks having salt solutions were stored safely at room temperature after covering them properly.

2.5. Synthesis of Silver NPs

To synthesize silver NPs, 50 mL of *Amomum subulatum* fruit extract with a concentration of 50 mg/mL was combined with a 50 mL aqueous solution containing silver nitrate salt (1 mM). This mixture was subjected to continuous stirring on a magnetic stirrer set at 250 rpm for a duration of 1 h at pH 7, facilitated by the gradual addition of 0.1N NaOH. The stirring process continued until the transparent $AgNO_3$ solution transitioned to a brownish-red. The entire biosynthesis procedure took place under diffused sunlight, as light exposure accelerates AgNP formation. Subsequently, the solution was subjected to centrifugation at 10,000 rpm to gather the sediment, which was then rinsed thrice with distilled water. The resulting product was lyophilized and stored at 4 °C for future applications.

2.6. Synthesis of Copper Oxide NPs

To synthesize copper oxide NPs, 50 mL of 50 mg/mL concentration of *Amomum subulatum* fruit extract was added to an aqueous solution of copper sulfate salt (0.05 M, 50 mL). The mixture was stirred with continuous heating at 70 °C on a magnetic stirrer at 250 rpm for 1 h at pH 7 using 0.1N NaOH until the color changed from blue ($CuSO_4 \cdot 5H_2O$) to brownish color. The color change confirmed the formation of NPs. The solution containing NPs was centrifuged at 7000 rpm, and the precipitate was collected and washed with distilled water thrice and dried at 70 °C in an oven for 6 h and stored for further use.

2.7. Optimisation of NPs

A UV–visible spectrophotometer was used to identify the formation of the AgNPs and CuONPs. The dried samples of AgNPs and CuONPs were dissolved in distilled water and taken in a small quartz cell for recording the spectra. To investigate the influence of metal salt solution concentration on NP production, a 1:1 ratio of silver nitrate salt solution (1 mM, 3 mM, and 5 mM) was added to a 50 mg/mL fruit extract solution. The mixture was kept on the magnetic stirrer and stirred at 250 rpm for 1 h. To determine the concentration effects of fruit extract, a fixed volume of 10 mL of 3 mM of $AgNO_3$ solution was added to different volumes of fruit extract (5 mL, 10 mL, 15 mL). They were kept on the magnetic stirrer and stirred at 250 rpm for 1 h. To study the effect of time on NP formation, 3 mM of silver salt solution was mixed with fruit extract in a ratio of 1:0.5. Three sets of NP solutions were created. One of the solutions was kept on the magnetic stirrer and stirred at 250 rpm

for 15 min, while the other two were stirred at 250 rpm for 30 min and 1 h, respectively. The same procedure was applied to CuONPs. To optimize the concentration of $CuSO_4$ salt solution (0.05 M, 0.1 M, and 0.2 M), the salt solution was mixed with the fruit extract in a ratio of 1:1 and stirred for 1 h at 70 °C and at 250 rpm. To determine the concentration of fruit extract, a fixed volume of 10 mL of 0.1 M $CuSO_4$ was added to different volumes of fruit extract (5 mL, 10 mL, 15 mL) and stirred magnetically for 1 h at 70 °C and 250 rpm. To optimize the time for the synthesis of NPs, 0.1 M solution of copper salt was mixed with the extract 50 mg/mL in a ratio 1:1 and stirred for 30 min at 250 rpm and 70 °C and the other two were stirred at 250 rpm and 70 °C at 1 h and 2 h respectively. All the NP solutions were studied using a UV-visible spectrometer (Shimadzu) to determine the synthesis of NPs.

2.8. Stability of Biosynthesized AgNPs and CuONPs

The stability of AgNPs and CuONPs was studied after the NPs were formed, centrifugation of the NPs was performed, and then the NPs were washed with distilled water thrice to remove any unreacted biological components to prevent agglomeration of NPs. To study the stability of NPs, the NP solutions were kept at room temperature at 30 °C, and the UV-visible spectra of NPs were recorded at different time intervals for up to 2 months [32].

2.9. Characterization

Various analytical methods were used to characterize the biosynthesized NPs. For determining the formation of NPs, the UV-visible absorption spectra of the NPs were recorded using a UV-visible spectrophotometer, Shimadzu UV-1800 series, with a 1 nm resolution. To determine the highest surface plasmon resonance, 2 mL of synthesized brownish-red solution of AgNPs and brown color of CuONPs were introduced to the quartz cuvette, and the spectrum was monitored at regular intervals of time. The presence of functional groups of the phytoconstituents, which are involved in the interaction with the nanoparticles for NPs synthesis and stability, was observed using Fourier transform infrared spectrometer Perkin Elmer Frontier FTIR-FIR Spectrophotometer (ATR) with 500–3500 cm^{-1} scanning range and 4 cm^{-1} resolution. The diffuse reflectance mode and 4 cm^{-1} resolution in KBr pellets are used for the experiment. In this study, 5 mg of completely dried metal NPs and 2 mL of plant aqueous extract were mixed with KBr, dried, and compressed to form KBr pellets and further spectra were obtained. Dynamic light scattering (DLS) and Zeta potential by Zetasizer nano series –Nano ZS 90 (Malvern Panalytical) was used to study the size distribution of the synthesized NPs in the colloidal solution [33]. The prepared NPs were dispersed in Milli–Q water with ultrasonification so that no extra peak appeared. The measurement was made in triplicate at a temperature of 24.5 °C, pH ≈ 6.5, refractive index of 1.33, and loading index of 2.45. Thereafter, the surface charge of the synthesized NPs was monitored by Zetasizer; 12 Zeta runs were taken with a count rate of 55.2 kcps. The crystalline nature of the synthesized NPs was determined by X-ray diffraction using an X-ray diffractometer (Bruker, D2-Phaser) having a CuK α source. The operating conditions used were 40 kV voltage and 30 mA current. Scanning was carried out in the range of 2θ values, and the crystalline size was calculated using Debye–Scherrer equation. Transmission electron microscope (TEM) JEOL 2010 LaB6 with W-source and point-to-point resolution of two, operating at 200 kV, were required to study the shape and size of the NPs. The prepared NPs were added into Milli-Q water and were sonicated for effective dispersion. A Few drops of the solution were kept on the TEM carbon grid, dried, and further analyzed.

2.10. Antibacterial Activity of Silver and Copper Oxide NPs by Well Diffusion Method

The antibacterial activity of silver and copper oxide NPs was studied by the agar well diffusion method. Soyabean Casein Digest Agar (SCDA) and Tryptone broth (Hi Media, Mumbai) were used as nutrient media. Gram-positive bacteria *Staphylococcus aureus* (ATCC 6538), *Bacillus subtilis* (ATCC 6633), and gram-negative bacteria *Escherichia coli* (ATCC 8739) culture suspensions were selected based on their pharmacological significance. Three Petri

plates were taken, and soybean SCDA media was poured into these petri plates. Bacterial cell suspensions were prepared and grown on tryptone broth, and cultures were incubated for 24 h at 37 °C. Cell density was adjusted to 1 × 10^6 cells/mL using 0.5 McFarland standards. Different bacterial cell suspensions were inoculated on different SCDA plates 90 mm by slowly revolving the plates for uniform distribution. When the agar solidified, eight wells were made in each petri plate with a cork borer, and each well was filled with different dilutions of AgNPs (50 µL, 100 µL) from 100 µg/mL of AgNPs, CuONPs (50 µL, 100 µL) from the concentration of 250 µg/mL, fruit extract (50 µL, 100 µL) from the concentration of 250 µg/mL. Gentamycin was taken as a positive control at a concentration of 50 µg/mL, and distilled water as a negative control. Plates were incubated at 37 °C for 24 h. After 24 h. zone of inhibition (longest diameter) in mm was recorded [34]. The experiment was performed in triplicate, and the diameter of the zone of inhibition was expressed as mean ± standard deviation (SD).

2.11. MTT Assay for Cytotoxicity Evaluation

The cell lines (human breast cells MCF-7, cervical cells HeLa) were obtained from the National Centre for Cell Science, Pune, India, for cytotoxicity assay. The cytotoxic activity of copper oxide and silver NPs on human cervical cells (HeLa) and human breast cells MCF-7 was evaluated using the MTT method. The stock cells were grown in DMEM (Dulbecco's Modified Eagle Medium) using 10% inactivated Fetal Bovine Serum in microtiter plates with 96 wells at 37 °C in a humidified environment of 5% CO_2. The cells were exposed to various doses of copper oxide (20 µg/mL, 50 µg/mL, 100 µg/mL, 250 µg/mL, 500 µg/mL, 1000 µg/mL) and silver NPs (10 µg/mL, 25 µg/mL, 50 µg/mL, 100 µg/mL, 200 µg/mL, 500 µg/mL) for 24 h. Doxorubicin (1.5 µg/mL, 3.1 µg/mL, 6.2 µg/mL, 12.5 µg/mL, 25 µg/mL µg/mL, 50 µg/mL, 100 µg/mL) was taken as a positive control. Cells with no NPs worked as a negative control. After the cells were treated with NPs, the medium was removed, 100 µL of MTT (5 mg/mL in phosphate buffer saline (PBS; pH 7.4) was added in all the wells for 4 h at 37 °C, and the formazan product formed was solubilized in DMSO. MTT assay employs MTT dye, which is changed to purple formazan by mitochondrial dehydrogenase enzymes of living cells. The microplate spectrophotometer was employed to assess the optical density at a wavelength of 570 nm [35]. The computation of cell viability percentage was accomplished using the provided equation:

$$\text{Cell viability (\%)} = \text{Absorbance of test}/\text{Absorbance of control} * 100$$

2.12. Statistical Evaluation

The average size of NPs was determined from the TEM and XRD spectra by using the Origin and Image J software. The antibacterial and cell viability IC_{50} results were presented as a mean ± standard deviation (n = 3). The statistical significance of differences between values of the treated and untreated (control) groups was evaluated by one-way ANOVA followed by Tukey's post hoc test (using the Graph Pad Prism 5.0 software). Differences with $p < 0.05$ were considered significant.

3. Results

3.1. Phytochemical Analysis

Screening of fruit extract of *Amomum subulatum* showed positive results for carbohydrates, flavonoids, saponins, tannins, proteins, glycosides, phenolic, and amino acids (Table 1).

Table 1. Preliminary phytochemical evaluation of *Amomum salbutum*.

Category	Test	Aqueous Extract
Carbohydrates	Molisch	+
Proteins	Millon	+
Flavonoids	Shinoda	+
Alkaloids	Dragendorff's	–
Saponins	Foam	+
Glycosides	Killer killani	+
Phenolic and tannins	Ferric chloride	+
Terpenoids	Salkowski	–
Amino acids	Ninhydrin	+

(–) Absent, (+) Present.

3.2. Visible Observation

The fruit extract of *Amomum subulatum* (Figure 1A) was used for the synthesis of silver and copper oxide NPs. (Figure 1B) The formation of silver and copper oxide NPs was depicted by the change in color of both precursor solutions. The visual color changed from light blue to brownish color, confirming the formation of copper oxide NPs. (Figure 1C) The color of the solution changed from transparent to reddish brown after adding the extract of *Amomum subulatum* to the silver nitrate salt solution due to the reduction of Ag^{+} ion to Ag^{0}, indicating the formation of AgNPs (Figure 1D).

Figure 1. (**A**) *Amomum sabulatum* fruit, (**B**) *Amomum sabulatum* fruit extract, (**C**) AgNPs in solution, (**D**) CuONPs in solution.

3.3. Ag and CuONPs Characterization

3.3.1. UV-Visible Analysis

The formation of NPs is easily determined by UV-visible spectroscopy. Surface plasmon resonance (SPR) peak of AgNPs was seen at λ 440 nm, and for CuONPs was observed at λ 245 nm in UV-visible spectra when fruit extract was added to the salt solutions which confirms the formation of NPs Figure 2A (I,II). The SPR of AgNPs and CuONPs was due to the interaction of surface electrons with incident light.

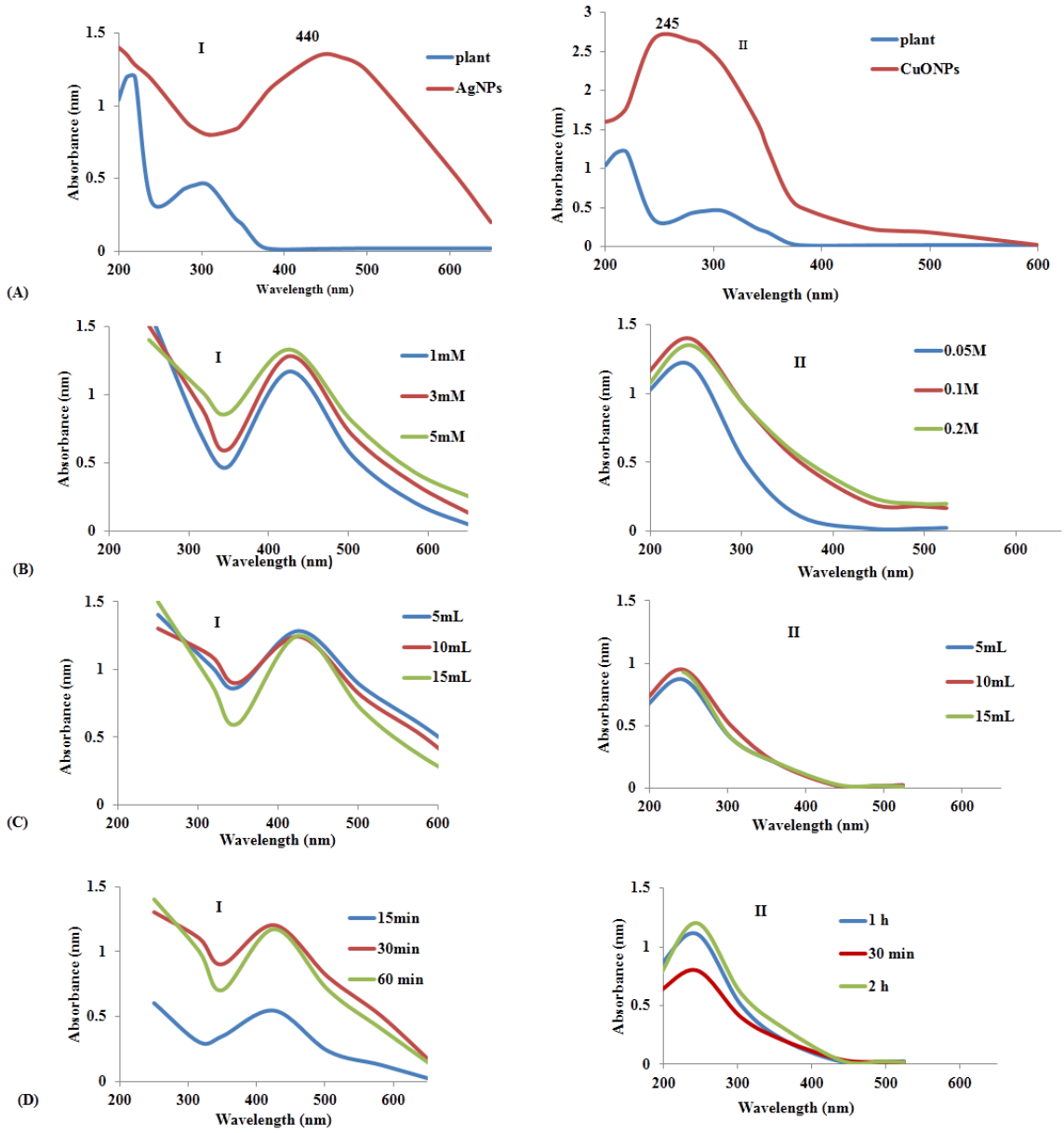

Figure 2. (**A**) The UV-visible spectrum of AgNPs solution (I) and CuONPs solution (II), (**B**) Effect of $AgNO_3$ concentration on the synthesis of AgNPs (I), the effect of $CuSO_4$ concentration on the synthesis of CuONPs (II), (**C**) the effect of *Amomum subulatum* fruit extract concentration on the synthesis of AgNPs (I), the effect of *Amomum subulatum* fruit extract concentration on the synthesis of and CuONPs (II), (**D**) effect of time interval on AgNPs synthesis (I) and effect of time interval on CuONPs synthesis (II).

The yield of AgNPs and CuONPs was optimized, varying the metal concentration, extract concentration, and time. Centrifugation of AgNPs and CuONPs solution was performed for different sets, and the NPs from each set were further dissolved in a fixed volume of distilled water, and the absorbance was measured. The yield calculated in terms of absorbance for AgNPs and CuONPs was maximum at 5 mM and 0.1 mM, respectively, as depicted in Figure 2B (I,II). Similarly, the concentration of the extract should be sufficient to reduce all the metal ions to increase the yield of NPs. Hence, an increase in the concentration of fruit extract causes an increase in the yield of NPs. In the case of AgNPs, where the salt solution and fruit extract were mixed in the ratio of 1:0.5, and for CuONPs, where the ratio

of copper salt and fruit extract was 1:1, a higher amount of NP formation was observed Figure 2C (I,II). Figure 2D (I,II) showed the effect of time interval on AgNPs and CuONPs synthesis and observed that In the case of AgNPs, an intense absorbance peak was found after 30 min, and for CuONPs after 2 h, and a further increase in time did not increase the intensity of the absorption peak. After noticing the UV-visible absorption peak of copper oxide and silver NPs, the above results were achieved.

3.3.2. Stability Study of AgNPs and CuONPs

The characteristic λ = 245 nm and λ = 440 nm peaks were observed for the synthesized CuONPs and AgNPs, indicating the stability of the synthesized NPs Figure 3. Thus, from the results, we can conclude that the synthesized CuONPs and AgNPs were quite stable, though a minor reduction in absorbance was observed for both NPs.

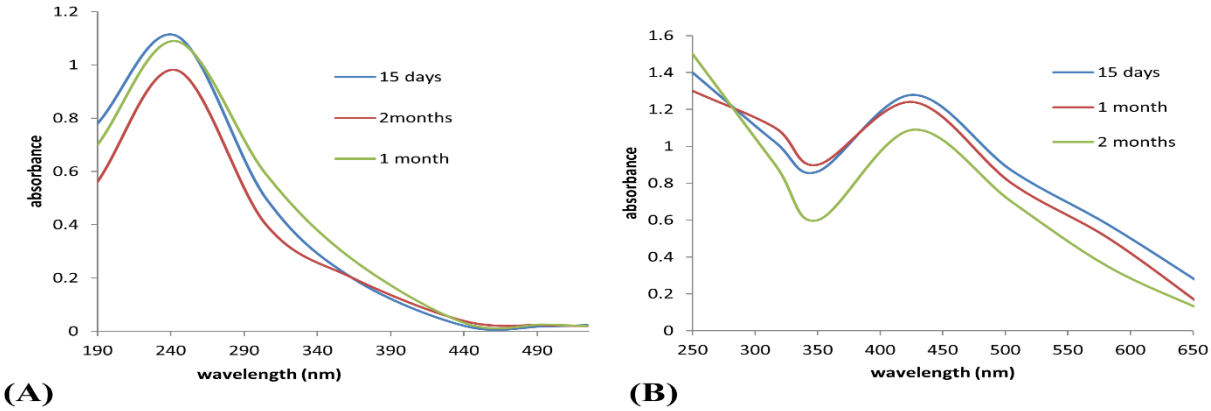

Figure 3. (**A**) Stability study of CuONPs under various time durations, (**B**) Stability study of AgNPs under various time durations.

3.3.3. Infrared Spectral Study and Powder XRD Diffraction Study

FTIR analysis was conducted to find out the possible phytoconstituents involved in metal NP synthesis and was responsible for stabilizing and capping the synthesized NPs. FTIR spectra of silver and copper oxide NPs were compared against the aqueous fruit extract of *Amomum subulatum*. It is apparent from Figure 4A that the silver and copper oxide NPs acquired bands that originated from the fruit extract. FTIR spectra of both the fruit extract Figure 4A (i) and the synthesized NPs showed similar peaks with minute shifts in the spectra.

IR spectra of AgNPs Figure 4A (ii) show a strong peak at 3321 cm^{-1}, which designates the stretching vibration of (O-H) of the phenolic group or amine functional group (N-H). The other strong band at 1636 cm^{-1} is attributed to the amide I band and -C=C- stretching vibration band. Likewise, in the spectrum of CuONPs, Figure 4A (iii), the band at 3323 cm^{-1} corresponds to the O-H stretching vibration of the phenolic group or amine (N-H) functional group. Strong bands at 1638 cm^{-1} correspond to the amide I band and -C=C- stretching vibration band. The peak at 1364 cm^{-1} corresponds to the -C-N- stretching band as well as the amide band of proteins in the fruit extract. Stretching vibration of ether functionality (C-O-C) was obtained at 1145 cm^{-1}, respectively [36].

The XRD graph shows the copper oxide and silver NP formation with their structural characteristics. The XRD diffraction pattern for silver NPs is presented in Figure 4B (i). The diffraction peaks were observed at 2θ values 38.19°, 44.35°, 64.51° and 77.39° relating to (111), (200), (220), (311) crystal planes. Using the Scherrer equation, the mean crystalline size of silver NPs was estimated to be 23.8 nm. XRD graph of CuONPs shows the intense peak at 2θ values 32.1°, 35.7°, 38.5°, 48.5°, 53.6°, 58.3°, 61.8°, 66.5° which corresponds to (110), (111), (200), (−202), (020), (202), (−113) and (022) respectively Figure 4B (ii). From the Scherrer equation, the mean crystal size of CuONPs was found to be 26.04 nm.

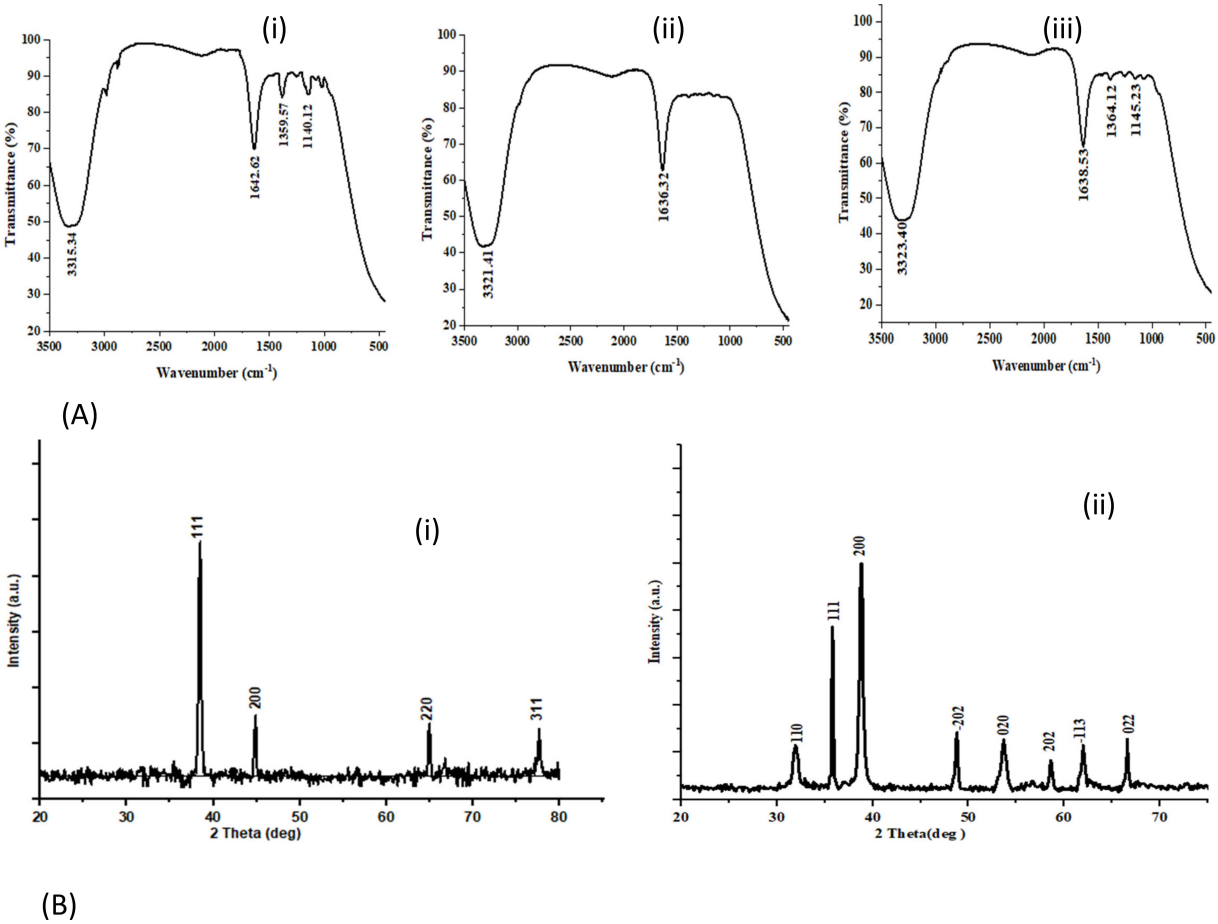

Figure 4. (**A**) FTIR spectrum of *Amomum sabulatum* fruit extract (i), AgNPs (ii) and CuONPs (iii) of *Amomum subulatum* fruit extract, (**B**) XRD spectrum of AgNPs and (i) CuONPs of *Amomum subulatum* fruit extract (ii).

3.3.4. Dynamic Light Scattering and Zeta Potential Analysis

DLS and Zeta potential analysis was conducted to determine the size and stability of NPs. As seen in Figure 5A, a single peak is seen at 92.97 nm, with the mean particle size distribution of silver NPs at 73.75 nm. The polydispersity index is 0.196, and the intensity of the peak recorded is 100%. A single peak is seen at 153 nm for copper oxide NPs, with the average size distribution being 103.5 nm. The polydispersity index was observed as 0.447, and the intensity of the peak recorded is 100% Figure 5B. The Zeta potential of AgNPs was observed to be −31.2 mV, and that of the CuONPs was −24 mV Figure 5C,D.

3.3.5. Transmission Electron Microscopy (TEM) Analysis

TEM analysis is conducted to determine the size and shape of the synthesized NPs. The TEM image Figure 6A,B of silver and copper oxide NPs revealed the shape of silver and CuONPs nanoparticles to be spherical, polydisperse, and non-uniformly distributed with some particles aggregated. Particle size distribution histogram of silver NPs and CuONPs of *Amomum subulatum* fruit extract Figure 6C,D. The mean particle size of silver NPs was found to be 20.6 nm and that of CuONPs 24.7 nm, which is very close to what is calculated from XRD.

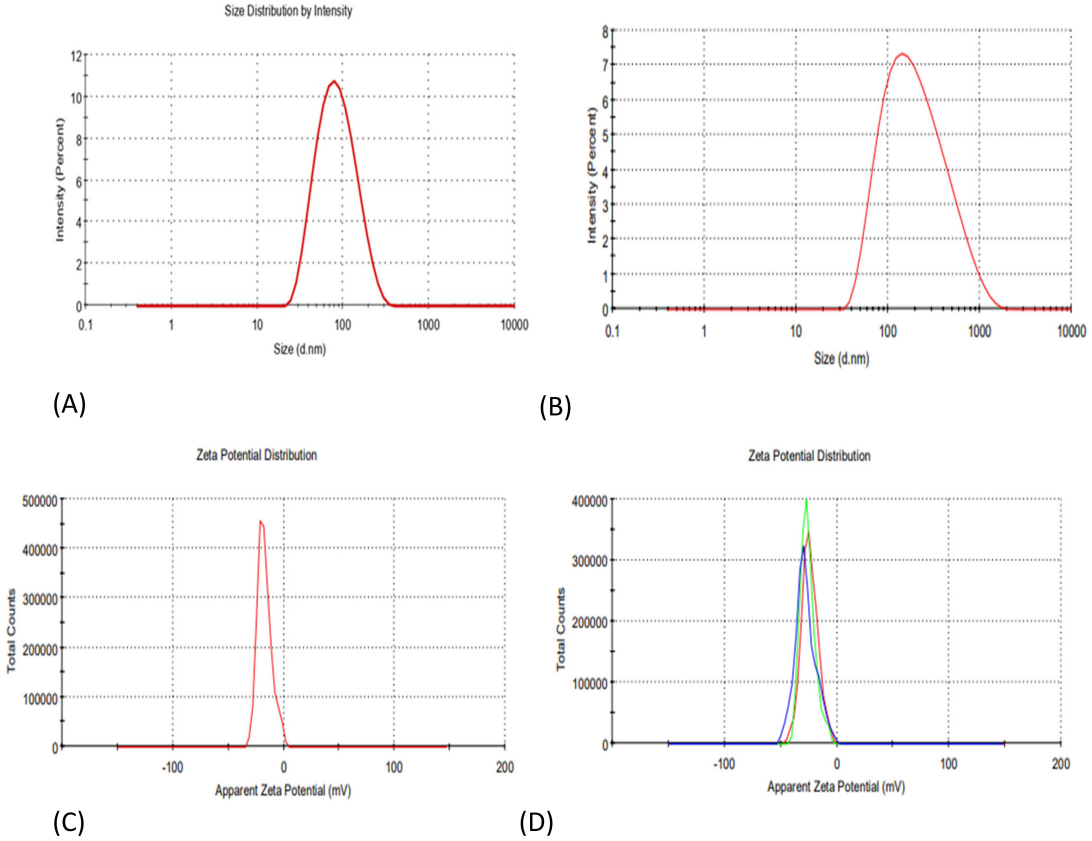

Figure 5. Particle size measurement of (**A**) AgNPs (**B**) CuONPs, Zeta potential measurement of (**C**) AgNPs (**D**) CuONPs.

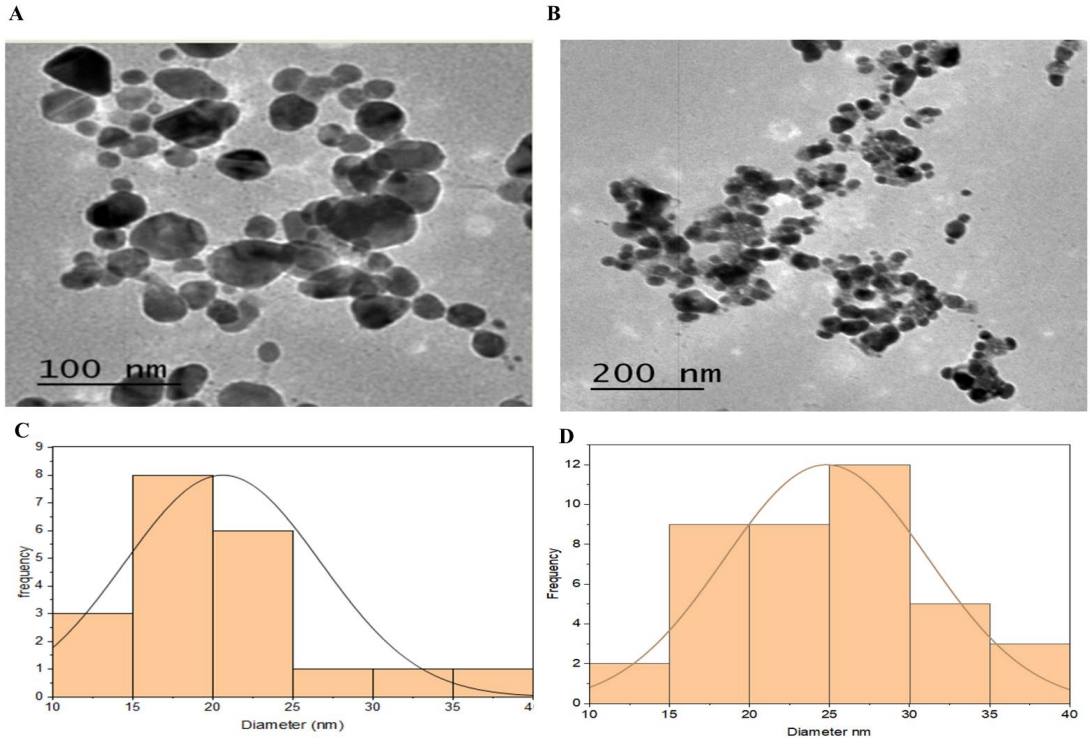

Figure 6. Surface morphology by TEM of (**A**) AgNPs, (**B**) CuONPs of *Amomum sabulatum* fruit extract, Particle size distribution histogram of (**C**) AgNPs, (**D**) CuONPs of *Amomum sabulatum* fruit extract.

3.3.6. Selected Area Electron Diffraction (SAED) Analysis

SAED pattern is another way to determine the crystalline nature of NPs. Figure 7A (i,ii) SAED pattern of silver NPs shows sharp concentric rings with a bright spot, which characterize the crystalline nature of the NPs originating from 111, 200, 220, and 311 planes. The SAED pattern of the CuONPs indicates sharp concentric circles with shiny spots, which characterize the nanocrystalline property of the sample originating from 111, 200, 202, and 113 planes.

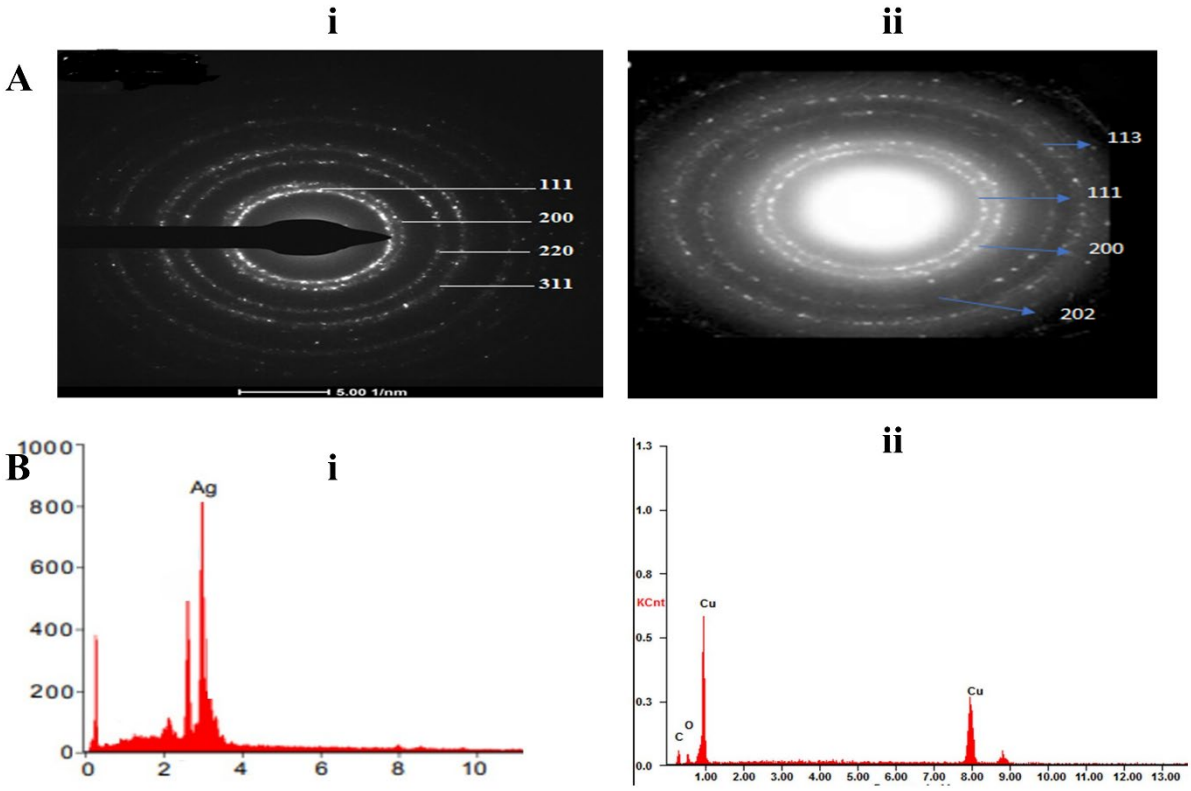

Figure 7. (**A**) SAED of AgNPs (i) and CuONPs (ii) of *Amomum subulatum* fruit extract, (**B**) EDS spectrum of AgNPs (i) and CuONPs of *Amomum subulatum* fruit extract (ii).

3.3.7. Energy Dispersive X-ray Spectroscopy Study

For further insight into the features of the biosynthesized AgNPs and CuONPs, the element present in the NPs was studied with the help of EDS. The energy dispersive spectrum of the samples which were obtained from TEM shows that the products consist of AgNPs and CuONPs of high purity, which also agrees with the results obtained from XRD analysis Figure 7B (i,ii).

3.4. Applications of Silver and Copper Oxide NPs

3.4.1. Antimicrobial Potential

The antimicrobial activity of silver and copper oxide NPs was tested using the well diffusion method, and the zone of inhibition (ZOI) was measured. The test was performed against gram-positive bacteria *B. subtilis* and *S. aureus* and gram-negative bacteria *E. coli.* As shown in Figure 8, the zone of inhibition (mm) was calculated after adding the drugs and then incubating at room temperature for 24 h. Table 2. The ZOI for *E. coli* was 19 mm, and for both *S. aureus* and *B. subtilis*, it was 18 mm when 100 µL of AgNP solution was used. For CuONPs 100 µL, the inhibition zone for *E. coli* was 14.5 mm and for both *S. aureus* and *B. subtilis* it was 14 mm. Crude plant extract did not show any antibacterial activity against any of these gram-positive and gram-negative bacteria at this particular concentration.

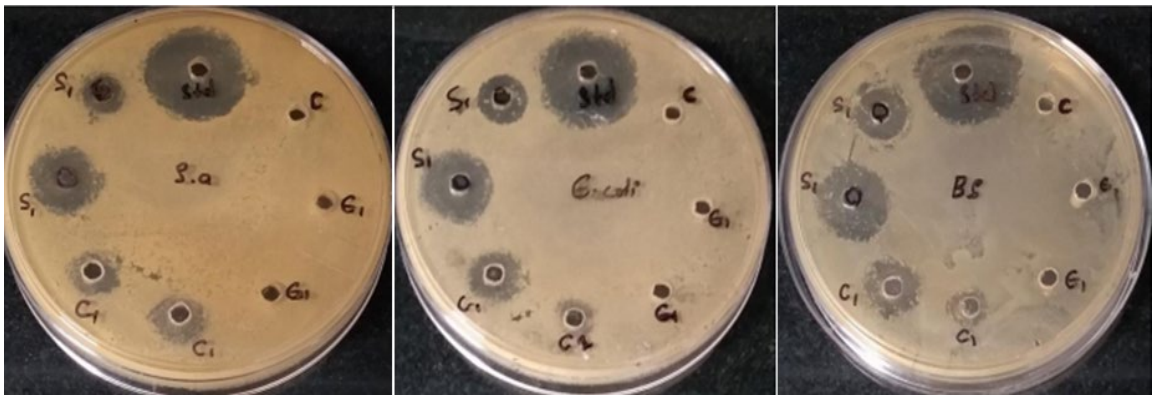

(**a**) (**b**) (**c**)

Figure 8. Antibacterial activity of fruit extract, AgNPs, and CuONPs prepared using *Amomum sabulatum* fruit against gram-positive bacteria *S. aureus* and *B. subtilis* (**a**,**c**) and gram-negative bacteria *E. coli* (**b**).

Table 2. Antibacterial testing using zone of inhibition analysis. Data represent mean ± SD (n = 3, $p < 0.05$).

Test Compounds	Volume per Well	*S. aureus*	*E. coli*	*B. subtilis*
		Zone of inhibition (mm)		
Distilled water (C)	50 µL	0	0	0
Plant extract (E)	100 µL	0	0	0
	50 µL	0	0	0
Gentamycin (Std)	50 µL	22 ± 0.1	22 ± 0.05	24 ± 0.12
AgNPs (S1)	100 µL	18 ± 0.5	19 ± 0.12	18 ± 0.02
	50 µL	11 ± 0.2	12 ± 0.05	13 ± 0.01
CuONPs (C1)	100 µL	14 ± 0.15	14.5 ± 0.05	14 ± 0.12
	50 µL	10 ± 0.2	10 ± 0.12	10 ± 0.11

3.4.2. In Vitro Cytotoxicity (MTT Assay)

The AgNPs and CuONPs treated HeLa and MCF-7 cells were analyzed through MTT assay after 24 h of adding various concentrations of 10–500 µg/mL for AgNPs and 20–1000 µg/mL for CuONPs. Figure 9A,B IC_{50} value of AgNPs was estimated to be 39.79 µg/mL and CuNPs was 83.89 µg/mL in MCF-7 cells, and IC_{50} values of AgNPs and CuNPs in HeLa cells were estimated to be 45.5 µg/mL and 97.07 µg/mL respectively. Figures 10 and 11 show the anticancer activity of AgNPs and CuONPs from dried fruit extract of *Amomum subulatum* against two cancer cell lines.

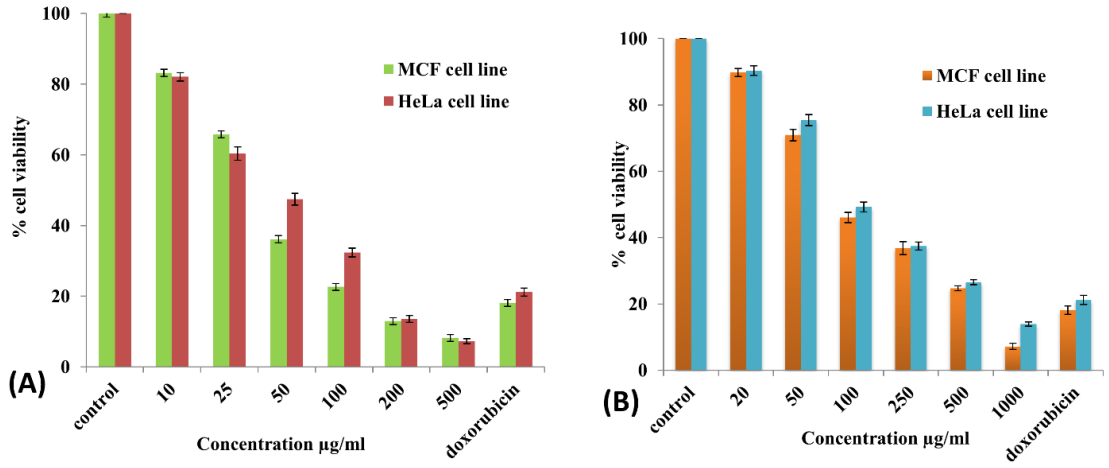

Figure 9. Representing the potency of AgNPs and CuONPs to inhibit half of the percentage of the biological process in a cell or an enzyme. (**A**) Anticancer activity of AgNPs against cancer cell line. (**B**) Anticancer activity of CuONPs against cancer cell line. Bars indicate mean ± SD (n = 3, $p < 0.05$).

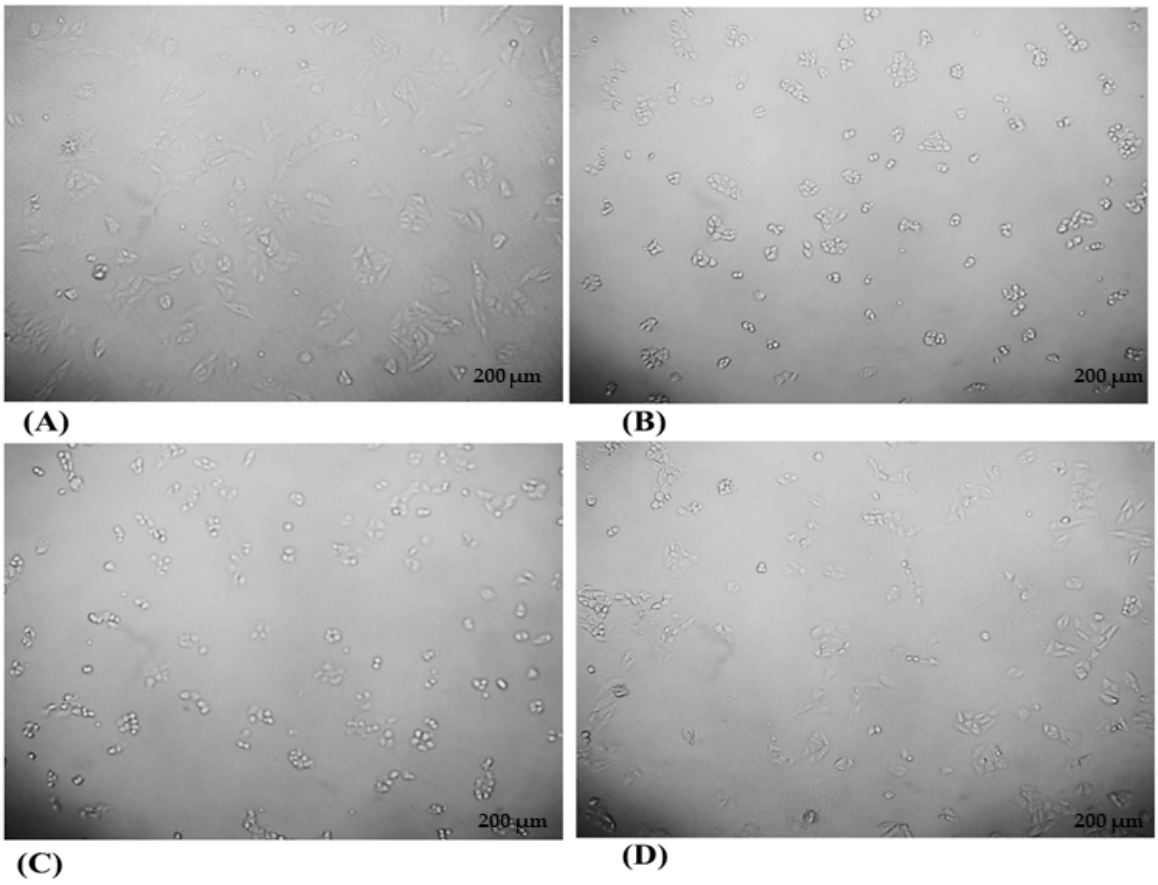

Figure 10. MCF-7 cell line treated with control (**A**) Doxorubicin (**B**) AgNPs (**C**), and CuONPs (**D**).

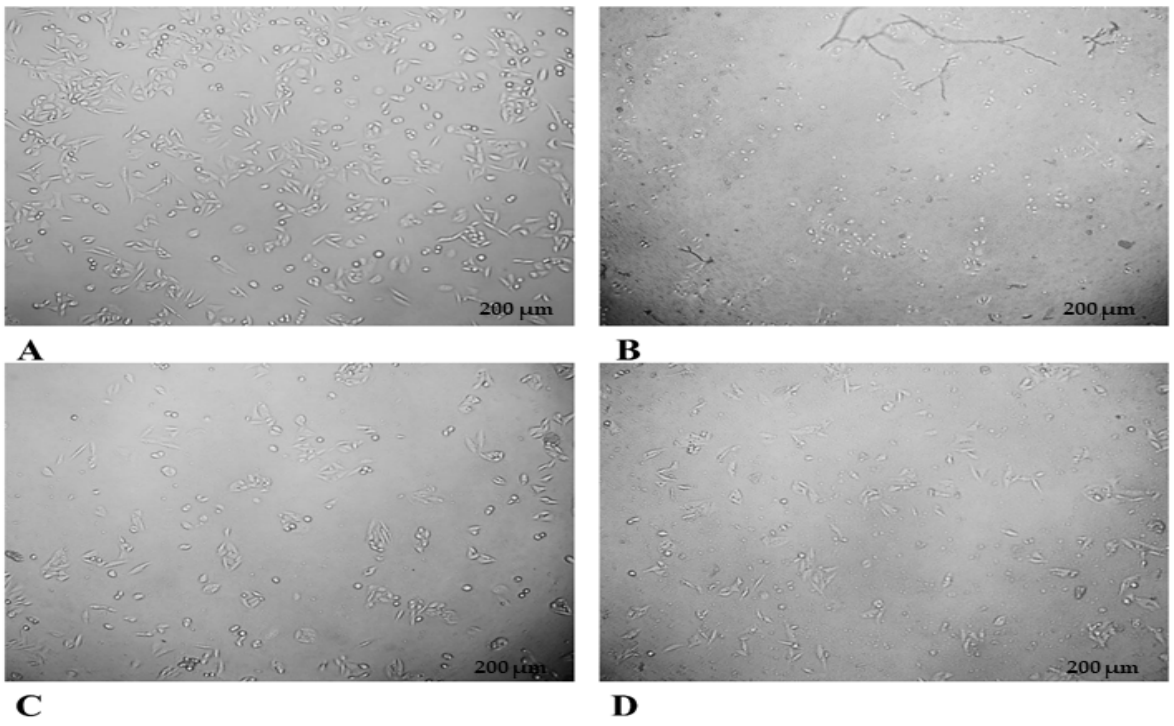

Figure 11. HeLa cell line treated with control (**A**) Doxorubicin (**B**), AgNPs (**C**) and CuONPs (**D**).

4. Discussion

Amongst the metal nanoparticles, silver and copper oxide NPs have drawn special attention because of their wide variety of applications. These metal nanoparticles exhibit good antibacterial and anticancer activity. The current study demonstrates a simple and eco-friendly synthesis of silver and copper oxide NPs using an aqueous extract of the dried fruit of *Amomum sabulatum.* The synthetic parameters were optimized to increase the yield of NPs; later, the characterization of the nanoparticles was performed using various analytical techniques using UV spectrophotometer, FT-IR, XRD, DLS, and TEM. The NPs were further subjected to antibacterial and anticancer activities by disc plate and MTT assay.

The first indication for the formation of AgNPs and CuONPs is provided by the color change of the metal salt solutions ($AgNO_3$ and $CuSO_4{\cdot}5H_2O$) when fruit extract of *Amomum subulatum* is added to them. The color of the solution changed from colorless to reddish brown after adding *Amomum subulatum* extract to the silver nitrate salt solution, which is due to the reduction of Ag^+ ion to Ag^0, indicating the formation of AgNPs. Prasad et al. [37] in his study also reported that in aqueous solutions, these nanoparticles gave out a reddish-brown color. For CuONPs, the color change of the precursor solution was from blue to brown when fruit extract was added to it. Nagajyothi et al. [38] showed that the color changes from blue to brownish black when plant extract is added to copper sulfate solution during the formation of copper oxide NPs.

The exact mechanism for the synthesis of metal NPs is not yet known, but there are several hypotheses that have been proposed by the researchers. As per one hypothesis, the first step in the synthesis of CuONPs is the formation of a polyphenolic complex with Cu^{+2} ion when the copper salt combines with plant extract, and then the reduction takes place, and Cu^{+2} is converted to Cu^0, which forms CuONPs through nucleation process.

$$Cu^{+2} + 2e \rightarrow Cu^0 + \text{Air } O_2 \rightarrow CuO$$

The phytochemicals present in the plant extract were used in the formation and stabilization of silver and copper oxide NPs. The process involved in the formation of metallic and metal oxide nanoparticles through biosynthesis encompasses the reduction of metal salts using biomolecules found within the plant extract, including polyphenols, flavonoids, proteins, tannins, as well as nucleation and subsequent nanoparticle growth. At last, the capping and stabilization take place [39,40]. Similar reports showed that in the green synthesis of CuONPs from different plant extracts of *Punica granatum* [41] and *Cissus arnotiana* [42], the phytocomponents such as flavonoids, tannins, phenolics act as reducing, capping, and stabilizing agents. The oscillation of surface electrons of metallic NPs generated SPR. The Surface plasmon resonance (SPR) peak of AgNPs was seen at λ 440 nm, and CuONPs was observed at λ 245 nm in UV-visible spectra. Mali et al. showed a characteristic peak at 254 nm for CuONPs [43]. Ruddaraju et al. reported the SPR peak at 430 nm for *Annona squamosa*-mediated silver NPs [44].

Copper oxide and silver NPs were optimized under different factors such as changing metal concentration, extract concentration, and time to obtain the highest yield of metal NPs. [45,46]. The bioactivity of NPs depends on various factors such as morphology, the functional group attached, surface charge, size of the NPs, and capping agent. A study reported that AgNPs, which have a small size and spherical shape, are more prone to release Ag^+ ions (which play a vital role in antibacterial activity) [47]. Keshari et al. biosynthesized AgNPs with a spherical shape and 20 nm in size using *Cestrum nocturnum* leaf extract. The MIC of biosynthesized AgNPs was reported as 16 µg/mL against *E. coli* [48]. Another study by Lee et al. showed that the anticancer activity of biologically synthesized gold NPs against HepG2 cells with IC_{50} value to be 127.1 µM for nanospheres and for nanostars shaped NPs the value was 81.8 µM and 22.7 µM for nanorod shaped nanoparticles [49]. Similarly, the silver and copper oxide NPs formed in the present study were spherical in shape with the mean particle size of 21 nm and 25 nm for silver and copper oxide

NPs, respectively, showing high antibacterial and anticancer activities comparable to the previously reported studies.

The bioactivity of green synthesized NPs also depends on the functional groups attached to the outer surface of NPs. Different bioactive have different efficacies, so metal NPs synthesized from different plant extracts will have differences in potency of biological activity. Gold NPs synthesized from two plants, *Carica papaya* and *Catharanthus roseus*, separately and evaluated against HepG2 cells for anticancer activity. NPs synthesized using *Carica papaya* were found to have IC_{50} of 100 µg/mL, and for *Catharanthus roseus*, the value was 150 µg/mL [50]. The silver NPs synthesized in the current study exert higher cytotoxicity against the HeLa (IC_{50} 46 µg/mL) and MCF-7 (IC_{50} 40µg/mL) cell lines, which can be attributed to higher proteins, amino acids, polyphenolics, and flavonoids which act as a capping agent and gets attached to the outer surface of metal NPs and exert synergistic cytotoxic effect with the metal NPs. Aggregation of metal NPs reduces the chances for the release of metal ion, and this could be fixed with the help of capping agents, which modifies the outer surface of metal NPs and thus can affect the efficacy of metal NPs [51]. Here in the present study, the proteins act as a capping agent and prevent the aggregation of the metal NPs synthesized, which is evident from the high value of Zeta potential −31 mV and −24 mV for silver and copper oxide NPs.

Time-dependent cytotoxicity of gold NPs was reported by Ashok Kumar et al. They reported the cytotoxicity of AuNPs synthesized from a plant extract of *Cajanus cajan* against HepG2 cells. The IC_{50} value after 24 h of treatment was found to be 6 µg/mL, and after 48 h, the IC_{50} was 2 µg/mL, showing time-dependent cytotoxicity [52].

UV-visible spectroscopy proved that the higher the concentration of the metal salt solution, the higher the number of NPs formed, which is determined by higher absorbance in UV-visible spectra [53]. Similarly, the concentration of the extract should be sufficient to reduce all the metal ions present as more of the phytochemicals were present for reduction.

FTIR analysis was conducted to determine the functional group present in the fruit extract *Amomum subulatum*, which could be responsible for the reduction and further stabilization of NPs. A strong peak of O-H stretching vibration is characteristic of phenols, or N-H stretching was attributed to the presence of proteins, peptides, and amino acids. The other strong amide I band is attributed to the stretch mode of the carbonyl group (C=O), which is attached to the amide linkage present on both the NPs. This amide I band may be due to the presence of proteins in the fruit extract. The protein might have coated and capped the synthesized AgNPs and CuONPs, prevented the agglomeration, and enhanced their stability. Osibe et al. showed absorbance bands at 3394, 1636, 1385, and 1074 cm^{-1}, which are very close to our findings [54]. Similar results were obtained by Jayaseelan et al.; peaks at 3427, 2925, 1629, 1387, and 1096 cm^{-1} were observed for CuONPs using *Tinospora cordifolia* leaf extract, which is consistent with our results [55]. From an FTIR spectral study, it can be estimated that the bioactive that were involved in the formation and stabilization of AgNPs and CuONPs could be phenolic, flavonoids, or proteins present in *Amomum subulatum* extract. According to the FTIR study by Iqbal et al. [56], silver nanoparticles bind to the carboxyl or amino groups of protein molecules. The amine (–NH), carboxyl (–C=O), and hydroxyl (–OH) groups of plant extracts are primarily involved in the synthesis of silver nanoparticles, as per one of the studies conducted [57].

The XRD pattern confirmed the crystalline nature of AgNPs with face-centered silver crystals respectively (JCPDS 00–004-0783), which is in agreement with the work reported previously by Waghmode et al. [58]. No extra peaks of other phases except that of the monoclinic structure for CuONPs were observed and were compared with the data from (JCPDS- 05–0661). The XRD pattern of CuONPs synthesized from plant extract shows similar diffraction peaks without significant shifts in the position of the peak [59]. This type of result was achieved from an *A. vera* leaf extract-mediated copper oxide NPs [60].

The biosynthesized NPs using *Amomum subulatum* extract were characterized using the Dynamic light scattering technique. Dynamic light scattering techniques determine the size of the particles by scattering light by the particles under Brownian motion [61]. The

size of the particles obtained is usually larger than that obtained by TEM analysis, as some of the bio-organic compounds may bind to the NPs, which does not occur in microscopy. The increase in size may also be due to the layering of the water molecules in the sample particles [62]. DLS study also showed that silver and copper oxide NPs were in the nano range. The average diameter of the particles in CuONPs was higher than that of AgNPs. Zeta potential analysis showed that the potential for silver NPs has a higher negative value than that of CuONPs. It is reported that Zeta potential with a negative value is because of the adsorption of hydroxyl ions. A higher negative value confers higher stability in the colloidal solution without aggregation [63]. Zeta potential is the potential taken at the shear plane that helps in evaluating the stability, adsorption studies, and surface morphology of the particles that are suspended [64]. The characterization of the sample was conducted using a Malvern Analytical instrument. A higher negative value of Zeta prevents agglomeration by increasing the electrostatic repulsion among the NPs [65]. The Zeta potential value obtained for AgNPs in the present study was well supported by the previous reports by Bhat et al., where the Zeta potential of AgNPs synthesized from *Ixora brachypoda* leaf extract was found to be −30.4 Mv [66]. In another study by Verma et al., the Zeta potential of CuONPs was found to be 16.4 mV, which is in agreement with the Zeta potential obtained in the present study [67].

The biosynthesized silver and copper oxide NPs in our study using *Amomum subulatum* extract, when characterized by TEM, were found to be spherical, polydisperse, and non-uniformly distributed with some CuONPs aggregated. Studies conducted by Devanesan et al. [68] also reported the TEM results for the particle size for AgNPs synthesized from the flower extract of *Abelmoschus esculentus* was in the range of 10 nm–25 nm, similar to the results obtained in the present study. Similarly, Rautela et al. [69] also reported that the AgNPs synthesized from *Tectona grandis* seeds extract have a mean particle size of 20 nm. A study conducted by Kasi et al. reported the results obtained by TEM analysis for the particle size of CuONPs synthesized using leaf extract of *Piper betle* were in the range of 20–40 nm [70].

The biosynthesized NPs were evaluated for antibacterial activity against gram-positive *S.aureus* and *B.subtilis* and gram-negative bacteria *E. coli.* ZOI was slightly more for gram-negative bacteria *E. coli* for both silver and copper oxide NPs. This can be attributed to the difference in the cell walls of both microbes. In a study conducted by Naveed et al., it was reported that silver NPs have more efficacy against gram-negative bacteria in comparison to gram-positive bacteria [71].

Results clearly show that AgNPs have better antimicrobial activity than CuONPs. A similar result was obtained by the research conducted by Verma et al., where silver and Copper oxide NPs were synthesized using leaf extract of *Catharanthus roseus*, and their antimicrobial activities were evaluated. It was found that the antimicrobial activity of the AgNPs was higher than that of the CuONPs [67].

The generalized mechanism of action of these NPs is that these NPs get attached to the cell wall and release Ag^{+} and Cu^{+2} ions, which change the structural composition of the cell wall of the bacteria by changing their penetrability and leading to the breaking of the cell wall. Their exceptionally small size, biocompatibility, and special morphologies kill various pathogenic bacteria. Reactive oxygen species, superoxide, and hydroxyl radicals formed by these NPs may be the reason for the death of bacteria [72,73].

In addition to this, the silver and copper oxide NPs also demonstrate excellent anticancer activity against MCF-7 and HeLa cell lines. The MTT results demonstrated the cytotoxic potential of AgNPs and CuONPs utilizing a colorimetric test to assess color changes (purple to yellow) in the presence of the enzyme mitochondrial succinate dehydrogenase in the cells. The cytotoxicity of nanoparticles is essentially determined by their size, shape, surface chemistry, particle aggregation, and contact duration [74,75]. In the present study, the anticancer activity of silver NPs was more than the copper oxide NPs against both cell lines. Previous reports supported this study about the inhibition concentration of silver NPs being 28 µg/mL [76]. Various mechanisms have been suggested to describe

the cytotoxic activity of metal NPs, like the formation of reactive oxygen species, caspase −3 activation, mitochondrial membrane permeabilization, and DNA damage leading to the apoptotic death of cancer cells. NPs of different sizes enter the cell by different mechanisms. Small NPs interact with caveolin receptors and enter the cell, whereas the large particles enter through clathrin-mediated endocytosis. Once inside the cell, they interact with certain proteins in the cytosol, trigger the generation of reactive oxygen species, and release metal ions, which then break the protein by binding with the SH group. The physiology of cells changes, and several signaling pathways are activated, leading to programmed cell death. Apoptosis is triggered by the NPs wherein the ROS generated results in depolarization of the mitochondrial membrane, releasing cytochrome c in the cytosol, which further leads to activation of caspase −9/3 apoptotic sequence and finally leads to cell death [77,78]. Cytotoxic potential in cancer cells can be distinguished by changes in shrinkage of the cell, change in filapodial length, detachment from the surface, and agglomeration of cells. It is represented in the study that the toxicity of the metal NPs shows a dose-dependent response in the tested cancer cells. An in-depth study is needed to understand the exact mechanism behind the anticancer activity of these synthesized silver and copper oxide NPs.

The antibacterial and anticancer activities of silver and Copper oxide NPs reported in this study are compared with the other plant-mediated silver and copper oxide NPs reported in the literature and are cited in Table 3. These findings clearly show that the present study showed greater zones of inhibition than the literature, highlighting the efficacy of *the Amomum sabulatum* fruit extract-mediated AgNPs and CuONPs. Similarly, the anticancer activity, which was not frequently performed by other researchers, had higher IC_{50} values than that found in our work, showing the high potential of silver and copper oxide NPs as cytotoxic agents. The present study also provides a comparative evaluation of the silver and copper oxide NPs.

Table 3. Comparative study of current research with previous studies.

Type of Metal NPs	Plant Extract	Antimicrobial Activity (Zone of Inhibition)	Anticancer Activity (IC_{50} Value)	Reference
AgNPs	*Amomum subulatum*	*S. aureus* (18 mm) *E. coli* (19 mm) *B. subtilis* (18 mm)	MCF Cells (39.79 µg/mL) HeLa cells (45.5 µg/mL)	Present study
CuONPs	*Amomum subulatum*	*S. aureus* (14 mm) *E. coli* (14.5 mm) *B. subtilis* (14 mm)	MCF Cells (83.89 µg/mL) HeLa cells (97.07 µg/mL)	Present study
CuONPs	*Catha edulis*	*S. aureus* (22 ± 0.01 mm) *genes* (24 ± 0.02 mm) *E. Coli* (32 ± 0.02 mm)		[79]
CuONPs	Allium sativum	*Escherichia coli* (7 mm) *S. aureus* (8 mm) *B. Subtilis* (7 mm) *S. phogenes* (7 mm)		[80]
AgNPs	*Parkia speciosa* leaves	*Escherichia coli* (9 mm) *S. aureus* (10 mm) *P. aeruginosa* (7 mm) *B. subtilis* (7 mm)		[81]
AgNPs	*Phoenix dactylifera* *Ferula asafetida* *Acacia nilotica* plant		46.15 ± 2.0 µg/mL 58.02 ± 2.1 µg/mL 69.73 ± 2.02 µg/mL	[82]
CuONPs	*Ficus religiosa*		200 µg/mL	[83]

5. Conclusions

In essence, this research introduces a simple, environmentally conscious, and effective approach to fabricating silver and copper oxide nanoparticles. These nanoparticles were generated through the utilization of an extract sourced from the *Amomum subulatum* fruit. The synthesis procedure was accompanied by a comprehensive analysis employing state-of-the-art techniques, including UV-visible spectroscopy, FTIR, TEM, DLS, and XRD. The resultant nanoparticles displayed a spherical morphology and maintained dimensions within the 100-nanometer scale. Notably, both the silver and copper oxide NPs exhibited the ability to eradicate both gram-positive and gram-negative bacterial strains. AgNP results show a larger zone of inhibition (ZOI) than CuONPs. The NPs further show promising anticancer activity. The cytotoxic activity of silver NPs against MCF-7 and HeLa cells was greater than the CuONPs. Conclusively, these Ag and CuONPs synthesized using *Amomum subulatum* fruit extract could function as better antimicrobial, anticancer, and also as a theranostics platform for biological applications such as antibacterial, antiviral, and anticancer.

6. Future Perspective and Limitations

Looking at the results, both the silver and copper oxide NPs have shown significant bactericidal and cytotoxic activity; hence further, studies can be carried out in the future on the molecular mechanism behind the cytotoxic effects of biosynthesized Ag and CuONPs on cancer cells in animal models. The reproducibility in the biosynthesis of metal nanoparticles has been recognized as one of the greatest challenges as small modifications of shape, size, and surface chemistry of the metal nanoparticles may drastically affect their stability, the distribution in biological fluid, and the interaction with biological systems.

Author Contributions: Conceptualization, S.D., R.D., R.P.S. and M.C.; methodology, S.D., R.D. and R.P.S.; formal analysis, S.D., R.D., T.V. and A.A.; investigation, S.D. and R.D.; resources, R.P.S.; writing—original draft preparation, S.D., R.D. and R.P.S.; writing—review and editing S.D., R.D., T.V., M.C., G.K., A.A., M.S.A., H.A.R. and M.A.-Z.; funding acquisition, M.S.A., H.A.R. and M.A.-Z.; supervision, R.D. All authors have read and agreed to the published version of the manuscript.

Funding: This work was supported and funded by the Deanship of Scientific Research at Imam Mohammad Ibn Saud Islamic University (IMSIU) (grant number IMSIU-RG23122).

Informed Consent Statement: Not applicable.

Data Availability Statement: Not applicable.

Conflicts of Interest: The authors declare no conflict of interest.

Sample Availability: Samples of the synthesized nanoparticles are available from the authors.

References

1. Singh, J.; Dutta, T.; Kim, K.-H.; Rawat, M.; Samddar, P.; Kumar, P. 'Green' Synthesis of Metals and Their Oxide Nanoparticles: Applications for Environmental Remediation. *J. Nanobiotechnol.* **2018**, *16*, 84. [CrossRef] [PubMed]
2. Nieto-Maldonado, A.; Bustos-Guadarrama, S.; Espinoza-Gomez, H.; Flores-López, L.Z.; Ramirez-Acosta, K.; Alonso-Nuñez, G.; Cadena-Nava, R.D. Green Synthesis of Copper Nanoparticles Using Different Plant Extracts and Their Antibacterial Activity. *J. Environ. Chem. Eng.* **2022**, *10*, 107130. [CrossRef]
3. Kumar, G.; Virmani, T.; Sharma, A.; Pathak, K. Codelivery of Phytochemicals with Conventional Anticancer Drugs in Form of Nanocarriers. *Pharmaceutics* **2023**, *15*, 889. [CrossRef] [PubMed]
4. Alhalmi, A.; Beg, S.; Almalki, W.H.; Alghamdi, S.; Kohli, K. Recent Advances in Nanotechnology-Based Targeted Therapeutics for Breast Cancer Management. *Curr. Drug Metab.* **2022**, *23*, 587–602. [CrossRef] [PubMed]
5. Alhalmi, A.; Beg, S.; Kohli, K.; Waris, M.; Singh, T. Nanotechnology Based Approach for Hepatocellular Carcinoma Targeting. *Curr. Drug Targets* **2021**, *22*, 779–792. [CrossRef]
6. Virmani, T.; Kumar, G.; Sharma, A.; Pathak, K.; Akhtar, M.S.; Afzal, O.; Altamimi, A.S.A. Amelioration of Cancer Employing Chitosan, Its Derivatives, and Chitosan-Based Nanoparticles: Recent Updates. *Polymers* **2023**, *15*, 2928. [CrossRef]
7. Khan, I.; Saeed, K.; Khan, I. Nanoparticles: Properties, Applications and Toxicities. *Arab. J. Chem.* **2019**, *12*, 908–931. [CrossRef]
8. Kumar, G.; Virmani, T.; Pathak, K.; Alhalmi, A. A Revolutionary Blueprint for Mitigation of Hypertension via Nanoemulsion. *BioMed Res. Int.* **2022**, *2022*, e4109874. [CrossRef] [PubMed]

9. Khursheed, R.; Dua, K.; Vishwas, S.; Gulati, M.; Jha, N.K.; Aldhafeeri, G.M.; Alanazi, F.G.; Goh, B.H.; Gupta, G.; Paudel, K.R.; et al. Biomedical Applications of Metallic Nanoparticles in Cancer: Current Status and Future Perspectives. *Biomed. Pharmacother.* **2022**, *150*, 112951. [CrossRef]
10. Virmani, T.; Kumar, G.; Virmani, R.; Sharma, A.; Pathak, K. Nanocarrier-Based Approaches to Combat Chronic Obstructive Pulmonary Disease. *Nanomedicine* **2022**, *17*, 1833–1854. [CrossRef]
11. Joudeh, N.; Linke, D. Nanoparticle Classification, Physicochemical Properties, Characterization, and Applications: A Comprehensive Review for Biologists. *J. Nanobiotechnol.* **2022**, *20*, 262. [CrossRef] [PubMed]
12. Hashem, A.H.; El-Sayyad, G.S. Antimicrobial and Anticancer Activities of Biosynthesized Bimetallic Silver-Zinc Oxide Nanoparticles (Ag-ZnO NPs) Using Pomegranate Peel Extract. *Biomass Conv. Bioref.* **2023**. [CrossRef]
13. Ali, A.; Zafar, H.; Zia, M.; Ul Haq, I.; Phull, A.R.; Ali, J.S.; Hussain, A. Synthesis, Characterization, Applications, and Challenges of Iron Oxide Nanoparticles. *NSA* **2016**, *9*, 49–67. [CrossRef] [PubMed]
14. Yousaf, A.; Waseem, M.; Javed, A.; Baig, S.; Ismail, B.; Baig, A.; Shahzadi, I.; Nawazish, S.; Zaman, I. Augmented Anticancer Effect and Antibacterial Activity of Silver Nanoparticles Synthesized by Using Taxus Wallichiana Leaf Extract. *PeerJ* **2022**, *10*, e14391. [CrossRef] [PubMed]
15. Andleeb, A.; Andleeb, A.; Asghar, S.; Zaman, G.; Tariq, M.; Mehmood, A.; Nadeem, M.; Hano, C.; Lorenzo, J.M.; Abbasi, B.H. A Systematic Review of Biosynthesized Metallic Nanoparticles as a Promising Anti-Cancer-Strategy. *Cancers* **2021**, *13*, 2818. [CrossRef] [PubMed]
16. Alruhaili, M.H.; Almuhayawi, M.S.; Gattan, H.S.; Alharbi, M.T.; Nagshabandi, M.K.; Jaouni, S.K.A.; Selim, S.; AbdElgawad, H. Insight into the Phytochemical Profile and Antimicrobial Activities of Amomum Subulatum and Amomum Xanthioides: An in Vitro and in Silico Study. *Front. Plant Sci.* **2023**, *14*, 1136961. [CrossRef] [PubMed]
17. Ihsan, M.; Niaz, A.; Rahim, A.; Zaman, M.I.; Arain, M.B.; Sirajuddin; Sharif, T.; Najeeb, M. Biologically Synthesized Silver Nanoparticle-Based Colorimetric Sensor for the Selective Detection of Zn^{2+}. *RSC Adv.* **2015**, *5*, 91158–91165. [CrossRef]
18. Ismail, M.; Xiangke, W.; Khan, A.A.; Khan, Q. Amomum Subalatum Leaf Extract Derived Silver Nanoparticles for Eco-Friendly Spectrophotometric Detection of Hg (II) Ions in Water. *Chem. Phys. Impact* **2023**, *6*, 100148. [CrossRef]
19. Ying, S.; Guan, Z.; Ofoegbu, P.C.; Clubb, P.; Rico, C.; He, F.; Hong, J. Green Synthesis of Nanoparticles: Current Developments and Limitations. *Environ. Technol. Innov.* **2022**, *26*, 102336. [CrossRef]
20. Purniawan, A.; Lusida, M.I.; Pujiyanto, R.W.; Nastri, A.M.; Permanasari, A.A.; Harsono, A.A.H.; Oktavia, N.H.; Wicaksono, S.T.; Dewantari, J.R.; Prasetya, R.R.; et al. Synthesis and Assessment of Copper-Based Nanoparticles as a Surface Coating Agent for Antiviral Properties against SARS-CoV-2. *Sci. Rep.* **2022**, *12*, 4835. [CrossRef]
21. Ghosh, S.; More, P.; Nitnavare, R.; Jagtap, S.; Chippalkatti, R.; Derle, A.; Kitture, R.; Asok, A.; Kale, S.; Ramanamurthy, B.; et al. Antidiabetic and Antioxidant Properties of Copper Nanoparticles Synthesized by Medicinal Plant Dioscorea Bulbifera. *J. Nanomed. Nanotechnol.* **2015**, *S6*, 7. [CrossRef]
22. Akintelu, S.A.; Bo, Y.; Folorunso, A.S. A Review on Synthesis, Optimization, Mechanism, Characterization, and Antibacterial Application of Silver Nanoparticles Synthesized from Plants. *J. Chem.* **2020**, *2020*, e3189043. [CrossRef]
23. Lee, S.H.; Jun, B.-H. Silver Nanoparticles: Synthesis and Application for Nanomedicine. *Int. J. Mol. Sci.* **2019**, *20*, 865. [CrossRef] [PubMed]
24. Ali, S.; Jalal, M.; Ahmad, H.; Sharma, D.; Ahmad, A.; Umar, K.; Khan, H. Green Synthesis of Silver Nanoparticles from Camellia Sinensis and Its Antimicrobial and Antibiofilm Effect against Clinical Isolates. *Materials* **2022**, *15*, 6978. [CrossRef] [PubMed]
25. Sadiq, M.U.; Shah, A.; Haleem, A.; Shah, S.M.; Shah, I. Eucalyptus Globulus Mediated Green Synthesis of Environmentally Benign Metal Based Nanostructures: A Review. *Nanomaterials* **2023**, *13*, 2019. [CrossRef] [PubMed]
26. Kumari, S.A.; Patlolla, A.K.; Madhusudhanachary, P. Biosynthesis of Silver Nanoparticles Using Azadirachta Indica and Their Antioxidant and Anticancer Effects in Cell Lines. *Micromachines* **2022**, *13*, 1416. [CrossRef] [PubMed]
27. Idrees, M.; Batool, S.; Kalsoom, T.; Raina, S.; Sharif, H.M.A.; Yasmeen, S. Biosynthesis of Silver Nanoparticles Using Sida Acuta Extract for Antimicrobial Actions and Corrosion Inhibition Potential. *Env. Technol.* **2019**, *40*, 1071–1078. [CrossRef] [PubMed]
28. Pant, D.R.; Pant, N.D.; Saru, D.B.; Yadav, U.N.; Khanal, D.P. Phytochemical Screening and Study of Antioxidant, Antimicrobial, Antidiabetic, Anti-Inflammatory and Analgesic Activities of Extracts from Stem Wood of Pterocarpus Marsupium Roxburgh. *J. Intercult. Ethnopharmacol.* **2017**, *6*, 170–176. [CrossRef]
29. Cyril, N.; George, J.B.; Joseph, L.; Raghavamenon, A.C.; Sylas, V.P. Assessment of Antioxidant, Antibacterial and Anti-Proliferative (Lung Cancer Cell Line A549) Activities of Green Synthesized Silver Nanoparticles from *Derris trifoliata*. *Toxicol. Res.* **2019**, *8*, 297–308. [CrossRef]
30. Jurado Gonzalez, P.; Sörensen, P.M. Characterization of Saponin Foam from Saponaria Officinalis for Food Applications. *Food Hydrocoll.* **2020**, *101*, 105541. [CrossRef]
31. Auwal, M.S.; Saka, S.; Mairiga, I.A.; Sanda, K.A.; Shuaibu, A.; Ibrahim, A. Preliminary Phytochemical and Elemental Analysis of Aqueous and Fractionated Pod Extracts of Acacia Nilotica (Thorn Mimosa). *Vet. Res. Forum.* **2014**, *5*, 95–100. [PubMed]
32. Bharadwaj, K.K.; Rabha, B.; Pati, S.; Choudhury, B.K.; Sarkar, T.; Gogoi, S.K.; Kakati, N.; Baishya, D.; Kari, Z.A.; Edinur, H.A. Green Synthesis of Silver Nanoparticles Using Diospyros Malabarica Fruit Extract and Assessments of Their Antimicrobial, Anticancer and Catalytic Reduction of 4-Nitrophenol (4-Np). *Nanomaterials* **2021**, *11*, 1999. [CrossRef] [PubMed]

33. Ahalwat, S.; Bhatt, D.C.; Rohilla, S.; Jogpal, V.; Sharma, K.; Virmani, T.; Kumar, G.; Alhalmi, A.; Alqahtani, A.S.; Noman, O.M.; et al. Mannose-Functionalized Isoniazid-Loaded Nanostructured Lipid Carriers for Pulmonary Delivery: In Vitro Prospects and In Vivo Therapeutic Efficacy Assessment. *Pharmaceuticals* **2023**, *16*, 1108. [CrossRef] [PubMed]
34. Balouiri, M.; Sadiki, M.; Ibnsouda, S.K. Methods for in Vitro Evaluating Antimicrobial Activity: A Review. *J. Pharm. Anal.* **2016**, *6*, 71–79. [CrossRef]
35. Mosmann, T. Rapid Colorimetric Assay for Cellular Growth and Survival: Application to Proliferation and Cytotoxicity Assays. *J. Immunol. Methods* **1983**, *65*, 55–63. [CrossRef] [PubMed]
36. Nakkala, J.R.; Mata, R.; Gupta, A.K.; Sadras, S.R. Biological Activities of Green Silver Nanoparticles Synthesized with Acorous Calamus Rhizome Extract. *Eur. J. Med. Chem.* **2014**, *85*, 784–794. [CrossRef] [PubMed]
37. Prasad, K.S.; Pathak, D.; Patel, A.; Dalwadi, P.; Prasad, R.; Patel, P.; Selvaraj, K. Biogenic Synthesis of Silver Nanoparticles Using Nicotiana Tobaccum Leaf Extract and Study of Their Antibacterial Effect. *Afr. J. Biotechnol.* **2011**, *10*, 8122–8130. [CrossRef]
38. Nagajyothi, P.C.; Muthuraman, P.; Sreekanth, T.V.M.; Kim, D.H.; Shim, J. Green Synthesis: In-Vitro Anticancer Activity of Copper Oxide Nanoparticles against Human Cervical Carcinoma Cells. *Arab. J. Chem.* **2017**, *10*, 215–225. [CrossRef]
39. Letchumanan, D.; Sok, S.P.M.; Ibrahim, S.; Nagoor, N.H.; Arshad, N.M. Plant-Based Biosynthesis of Copper/Copper Oxide Nanoparticles: An Update on Their Applications in Biomedicine, Mechanisms, and Toxicity. *Biomolecules* **2021**, *11*, 564. [CrossRef]
40. Vincent, J.; Lau, K.S.; Evyan, Y.C.Y.; Chin, S.X.; Sillanpää, M.; Chia, C.H. Biogenic Synthesis of Copper-Based Nanomaterials Using Plant Extracts and Their Applications: Current and Future Directions. *Nanomaterials* **2022**, *12*, 3312. [CrossRef]
41. Vidovix, T.B.; Quesada, H.B.; Januário, E.F.D.; Bergamasco, R.; Vieira, A.M.S. Green Synthesis of Copper Oxide Nanoparticles Using Punica Granatum Leaf Extract Applied to the Removal of Methylene Blue. *Mater. Lett.* **2019**, *257*, 126685. [CrossRef]
42. Rajeshkumar, S.; Menon, S.; Venkat Kumar, S.; Tambuwala, M.M.; Bakshi, H.A.; Mehta, M.; Satija, S.; Gupta, G.; Chellappan, D.K.; Thangavelu, L.; et al. Antibacterial and Antioxidant Potential of Biosynthesized Copper Nanoparticles Mediated through Cissus Arnotiana Plant Extract. *J. Photochem. Photobiol. B Biol.* **2019**, *197*, 111531. [CrossRef] [PubMed]
43. Chand Mali, S.; Raj, S.; Trivedi, R. Biosynthesis of Copper Oxide Nanoparticles Using Enicostemma Axillare (Lam.) Leaf Extract. *Biochem. Biophys. Rep.* **2019**, *20*, 100699. [CrossRef]
44. Ruddaraju, L.K.; Pallela, P.N.V.K.; Pammi, S.V.N.; Padavala, V.S.; Kolapalli, V.R.M. Synergetic Antibacterial and Anticarcinogenic Effects of Annona Squamosa Leaf Extract Mediated Silver Nano Particles. *Mater. Sci. Semicond. Process.* **2019**, *100*, 301–309. [CrossRef]
45. Souri, M.; Hoseinpour, V.; Ghaemi, N.; Shakeri, A. Procedure Optimization for Green Synthesis of Manganese Dioxide Nanoparticles by Yucca Gloriosa Leaf Extract. *Int. Nano Lett.* **2019**, *9*, 73–81. [CrossRef]
46. Kumar, S.V.; Bafana, A.P.; Pawar, P.; Faltane, M.; Rahman, A.; Dahoumane, S.A.; Kucknoor, A.; Jeffryes, C.S. Optimized Production of Antibacterial Copper Oxide Nanoparticles in a Microwave-Assisted Synthesis Reaction Using Response Surface Methodology. *Colloids Surf. A Physicochem. Eng. Asp.* **2019**, *573*, 170–178. [CrossRef]
47. Talank, N.; Morad, H.; Barabadi, H.; Mojab, F.; Amidi, S.; Kobarfard, F.; Mahjoub, M.A.; Jounaki, K.; Mohammadi, N.; Salehi, G.; et al. Bioengineering of Green-Synthesized Silver Nanoparticles: In Vitro Physicochemical, Antibacterial, Biofilm Inhibitory, Anticoagulant, and Antioxidant Performance. *Talanta* **2022**, *243*, 123374. [CrossRef]
48. Keshari, A.K.; Srivastava, R.; Singh, P.; Yadav, V.B.; Nath, G. Antioxidant and Antibacterial Activity of Silver Nanoparticles Synthesized by Cestrum Nocturnum. *J. Ayurveda Integr. Med.* **2020**, *11*, 37–44. [CrossRef]
49. Lee, Y.J.; Ahn, E.Y.; Park, Y. Shape-Dependent Cytotoxicity and Cellular Uptake of Gold Nanoparticles Synthesized Using Green Tea Extract. *Nanoscale Res. Lett.* **2019**, *14*, 1–14. [CrossRef]
50. Barabadi, H.; Webster, T.J.; Vahidi, H.; Sabori, H.; Damavandi Kamali, K.; Jazayeri Shoushtari, F.; Mahjoub, M.A.; Rashedi, M.; Mostafavi, E.; Cruz, D.M.; et al. Green Nanotechnology-Based Gold Nanomaterials for Hepatic Cancer Therapeutics: A Systematic Review. *Iran. J. Pharm. Res. IJPR* **2020**, *19*, 3–17. [CrossRef]
51. Ahmad, S.A.; Das, S.S.; Khatoon, A.; Ansari, M.T.; Afzal, M.; Hasnain, M.S.; Nayak, A.K. Bactericidal Activity of Silver Nanoparticles: A Mechanistic Review. *Mater. Sci. Energy Technol.* **2020**, *3*, 756–769. [CrossRef]
52. Ashokkumar, T.; Prabhu, D.; Geetha, R.; Govindaraju, K.; Manikandan, R.; Arulvasu, C.; Singaravelu, G. Apoptosis in Liver Cancer (HepG2) Cells Induced by Functionalized Gold Nanoparticles. *Colloids Surf. B Biointerfaces* **2014**, *123*, 549–556. [CrossRef] [PubMed]
53. Cuong, H.N.; Pansambal, S.; Ghotekar, S.; Oza, R.; Thanh Hai, N.T.; Viet, N.M.; Nguyen, V.-H. New Frontiers in the Plant Extract Mediated Biosynthesis of Copper Oxide (CuO) Nanoparticles and Their Potential Applications: A Review. *Environ. Res.* **2022**, *203*, 111858. [CrossRef] [PubMed]
54. Osibe, D.A.; Aoyagi, H. A Novel Strategy for the Synthesis of Gold Nanoparticles with Catharanthus Roseus Cell Suspension Culture. *Mater. Lett.* **2019**, *238*, 317–320. [CrossRef]
55. Jayaseelan, C.; Abdulhaq, A.; Ragavendran, C.; Mohan, S. Phytoconstituents Assisted Biofabrication of Copper Oxide Nanoparticles and Their Antiplasmodial, and Antilarval Efficacy: A Novel Approach for the Control of Parasites. *Molecules* **2022**, *27*, 8269. [CrossRef] [PubMed]
56. Iqbal, N.; Iqubal, S.M.S.; Khan, A.A.; Mohammed, T.; Alshabi, A.M.; Aazam, E.S.; Rafiquee, M.Z.A. Effect of CTABr (Surfactant) on the Kinetics of Formation of Silver Nanoparticles by Amla Extract. *J. Mol. Liq.* **2021**, *329*, 115537. [CrossRef]
57. Tuama, A.A.; Mohammed, A.A. Phytochemical Screening and in Vitro Antibacterial and Anticancer Activities of the Aqueous Extract of Cucumis Sativus. *Saudi J. Biol. Sci.* **2019**, *26*, 600–604. [CrossRef]

58. Waghmode, S.; Chavan, P.; Kalyankar, V.; Dagade, S. Synthesis of Silver Nanoparticles Using *Triticum Aestivum* and Its Effect on Peroxide Catalytic Activity and Toxicology. *J. Chem.* **2013**, *2013*, 265864. [CrossRef]
59. Sundaramurthy, N.; Parthiban, C. Biosynthesis of Copper Oxide Nanoparticles Using Pyrus Pyrifolia Leaf Extract and Evolve the Catalytic Activity. *Int. Res. J. Eng. Technol.* **2015**, *2*, 332–338.
60. Kumar, P.P.N.V.; Shameem, U.; Kollu, P.; Kalyani, R.L.; Pammi, S.V.N. Green Synthesis of Copper Oxide Nanoparticles Using Aloe Vera Leaf Extract and Its Antibacterial Activity Against Fish Bacterial Pathogens. *BioNanoScience* **2015**, *5*, 135–139. [CrossRef]
61. Khatua, A.; Prasad, A.; Priyadarshini, E.; Patel, A.K.; Naik, A.; Saravanan, M.; Barabadi, H.; Ghosh, L.; Paul, B.; Paulraj, R.; et al. Emerging Antineoplastic Plant-Based Gold Nanoparticle Synthesis: A Mechanistic Exploration of Their Anticancer Activity Toward Cervical Cancer Cells. *J. Clust. Sci.* **2019**, *31*, 1329–1340. [CrossRef]
62. Mali, S.C.; Dhaka, A.; Githala, C.K.; Trivedi, R. Green Synthesis of Copper Nanoparticles Using Celastrus Paniculatus Willd. Leaf Extract and Their Photocatalytic and Antifungal Properties. *Biotechnol. Rep.* **2020**, *27*, e00518. [CrossRef]
63. Thirumagal, N.; Jeyakumari, A.P. Structural, Optical and Antibacterial Properties of Green Synthesized Silver Nanoparticles (AgNPs) Using Justicia Adhatoda L. Leaf Extract. *J. Clust. Sci.* **2020**, *31*, 487–497. [CrossRef]
64. Alhalmi, A.; Amin, S.; Khan, Z.; Beg, S.; Al, O.; Saleh, A.; Kohli, K. Nanostructured Lipid Carrier-Based Codelivery of Raloxifene and Naringin: Formulation, Optimization, In Vitro, Ex Vivo, In Vivo Assessment, and Acute Toxicity Studies. *Pharmaceutics* **2022**, *14*, 1771. [CrossRef] [PubMed]
65. Kumar, G.; Virmani, T.; Pathak, K.; Kamaly, O.A.; Saleh, A. Central Composite Design Implemented Azilsartan Medoxomil Loaded Nanoemulsion to Improve Its Aqueous Solubility and Intestinal Permeability: In Vitro and Ex Vivo Evaluation. *Pharmaceuticals* **2022**, *15*, 1343. [CrossRef] [PubMed]
66. Bhat, M.; Chakraborty, B.; Kumar, R.S.; Almansour, A.I.; Arumugam, N.; Kotresha, D.; Pallavi, S.S.; Dhanyakumara, S.B.; Shashiraj, K.N.; Nayaka, S. Biogenic Synthesis, Characterization and Antimicrobial Activity of Ixora Brachypoda (DC) Leaf Extract Mediated Silver Nanoparticles. *J. King Saud Univ.–Sci.* **2021**, *33*, 101296. [CrossRef]
67. Verma, A.; Bharadvaja, N. Plant-Mediated Synthesis and Characterization of Silver and Copper Oxide Nanoparticles: Antibacterial and Heavy Metal Removal Activity. *J. Clust. Sci.* **2022**, *33*, 1697–1712. [CrossRef]
68. Devanesan, S.; AlSalhi, M.S. Green Synthesis of Silver Nanoparticles Using the Flower Extract of Abelmoschus Esculentus for Cytotoxicity and Antimicrobial Studies. *Int. J. Nanomed.* **2021**, *16*, 3343–3356. [CrossRef]
69. Rautela, A.; Rani, J.; Debnath (Das), M. Green Synthesis of Silver Nanoparticles from Tectona Grandis Seeds Extract: Characterization and Mechanism of Antimicrobial Action on Different Microorganisms. *J. Anal. Sci. Technol.* **2019**, *10*, 5. [CrossRef]
70. Kasi, S.D.; Ramasamy, J.M.; Nagaraj, D.; Santiyagu, V.; Ponraj, J.S. Biogenic Synthesis of Copper Oxide Nanoparticles Using Leaf Extracts of Cissus Quadrangularis and Piper Betle and Its Antibacterial Effects. *Micro Nano Lett.* **2021**, *16*, 419–424. [CrossRef]
71. Naveed, M.; Bukhari, B.; Aziz, T.; Zaib, S.; Mansoor, M.A.; Khan, A.A.; Shahzad, M.; Dablool, A.S.; Alruways, M.W.; Almalki, A.A.; et al. Green Synthesis of Silver Nanoparticles Using the Plant Extract of Acer Oblongifolium and Study of Its Antibacterial and Antiproliferative Activity via Mathematical Approaches. *Molecules* **2022**, *27*, 4226. [CrossRef] [PubMed]
72. Bhavyasree, P.G.; Xavier, T.S. Green Synthesised Copper and Copper Oxide Based Nanomaterials Using Plant Extracts and Their Application in Antimicrobial Activity: Review. *Curr. Res. Green Sustain. Chem.* **2022**, *5*, 100249. [CrossRef]
73. Bouafia, A.; Laouini, S.E.; Ouahrani, M.R. A Review on Green Synthesis of CuO Nanoparticles Using Plant Extract and Evaluation of Antimicrobial Activity A Review on Green Synthesis of CuO Nanoparticles Using Plant Extract and Evaluation of Antimicrobial Activity. *Asian J. Res. Chem.* **2020**, *13*, 65–70. [CrossRef]
74. Park, M.V.D.Z.; Neigh, A.M.; Vermeulen, J.P.; de la Fonteyne, L.J.J.; Verharen, H.W.; Briedé, J.J.; van Loveren, H.; de Jong, W.H. The Effect of Particle Size on the Cytotoxicity, Inflammation, Developmental Toxicity and Genotoxicity of Silver Nanoparticles. *Biomaterials* **2011**, *32*, 9810–9817. [CrossRef] [PubMed]
75. Sahu, N.; Soni, D.; Chandrashekhar, B.; Satpute, D.B.; Saravanadevi, S.; Sarangi, B.K.; Pandey, R.A. Synthesis of Silver Nanoparticles Using Flavonoids: Hesperidin, Naringin and Diosmin, and Their Antibacterial Effects and Cytotoxicity. *Int. Nano Lett.* **2016**, *6*, 173–181. [CrossRef]
76. Gomathi, A.C.; Xavier Rajarathinam, S.R.; Mohammed Sadiq, A.; Rajeshkumar, S. Anticancer Activity of Silver Nanoparticles Synthesized Using Aqueous Fruit Shell Extract of Tamarindus Indica on MCF-7 Human Breast Cancer Cell Line. *J. Drug Deliv. Sci. Technol.* **2020**, *55*, 101376. [CrossRef]
77. Thangam, R.; Senthilkumar, D.; Suresh, V.; Sathuvan, M.; Sivasubramanian, S.; Pazhanichamy, K.; Gorlagunta, P.K.; Kannan, S.; Gunasekaran, P.; Rengasamy, R.; et al. Induction of ROS-Dependent Mitochondria-Mediated Intrinsic Apoptosis in MDA-MB-231 Cells by Glycoprotein from Codium Decorticatum. *J. Agric. Food Chem.* **2014**, *62*, 3410–3421. [CrossRef] [PubMed]
78. Takahashi, A.; Masuda, A.; Sun, M.; Centonze, V.E.; Herman, B. Oxidative Stress-Induced Apoptosis Is Associated with Alterations in Mitochondrial Caspase Activity and Bcl-2-Dependent Alterations in Mitochondrial PH (PHm). *Brain Res. Bull.* **2004**, *62*, 497–504. [CrossRef]
79. Andualem, W.W.; Sabir, F.K.; Mohammed, E.T.; Belay, H.H.; Gonfa, B.A. Synthesis of Copper Oxide Nanoparticles Using Plant Leaf Extract of *Catha Edulis* and Its Antibacterial Activity. *J. Nanotechnol.* **2020**, *2020*, e2932434. [CrossRef]
80. Velsankar, K.; Aswin Kumar, R.M.; Preethi, R.; Muthulakshmi, V.; Sudhahar, S. Green Synthesis of CuO Nanoparticles via Allium Sativum Extract and Its Characterizations on Antimicrobial, Antioxidant, Antilarvicidal Activities. *J. Environ. Chem. Eng.* **2020**, *8*, 104123. [CrossRef]

81. Ravichandran, V.; Vasanthi, S.; Shalini, S.; Shah, S.A.A.; Tripathy, M.; Paliwal, N. Green Synthesis, Characterization, Antibacterial, Antioxidant and Photocatalytic Activity of Parkia Speciosa Leaves Extract Mediated Silver Nanoparticles. *Results Phys.* **2019**, *15*, 102565. [CrossRef]
82. Mohammed, A.E.; Al-Qahtani, A.; Al-Mutairi, A.; Al-Shamri, B.; Aabed, K.F. Antibacterial and Cytotoxic Potential of Biosynthesized Silver Nanoparticles by Some Plant Extracts. *Nanomaterials* **2018**, *8*, 382. [CrossRef] [PubMed]
83. Sankar, R.; Maheswari, R.; Karthik, S.; Shivashangari, K.S.; Ravikumar, V. Anticancer Activity of Ficus Religiosa Engineered Copper Oxide Nanoparticles. *Mater. Sci. Eng. C* **2014**, *44*, 234–239. [CrossRef] [PubMed]